FINAL

MONO LAKE AIR QUALITY MODEL EVALUATION STUDY

Prepared for:

Great Basin Unified APCD
Bishop, CA

TRC Project No. 9616

November 11, 1991

TRC
Environmental Consultants

21907 64th Avenue. W.
Suite 230
Mountlake Terrace, WA 98043

(206) 778-5003

A TRC Company

TABLE OF CONTENTS

MONO LAKE AIR QUALITY MODEL EVALUATION STUDY

LIST OF TABLES

LIST OF FIGURES

MONO LAKE AIR QUALITY MODEL EVALUATION STUDY

1.0 Introduction

The Mono Lake Evaluation Study was conducted to evaluate dispersion modeling techniques for simulation of wind-blown PM_{10} emissions from the exposed shores of Mono Lake. Ambient monitoring within Mono Basin has indicated that both the California Ambient Air Quality Standard (CAAQS) and the National Ambient Air Quality Standard (NAAQS) for 24-hour PM_{10} concentration have been exceeded at several monitoring locations. These episodes were accompanied by high winds and visual evidence suggests that wind-blown dust emissions from the exposed shores of Mono Lake were responsible (Cox, 1990). The present study was initiated in order to evaluate dispersion modeling tools that could be applied to investigate these wind-blown dust events. Dispersion model simulations can be used to supplement the ambient data by providing predictions at receptor locations and for times outside of the monitoring network. In addition, dispersion modeling can be applied as a tool to aid in the management of the air basin, for the assessment of mitigating measures, and for PM_{10} source apportionment.

The objective of the Mono Lake Evaluation Study was to assess dispersion modeling techniques for the prediction of PM_{10} concentrations during high wind events. The study included the evaluation of two dispersion models and two alternative methods for the estimation of wind-blown PM_{10} emissions. Section 2 presents an overview of the dispersion models and emission factors that were selected for the study. The wind-blown dust emission algorithms included in the study were developed by Great Basin Unified Air Pollution Control District (GBUAPCD) and the Midwest Research Institute (MRI) based on interpretations of wind tunnel tests conducted at Mono Lake during the late summer of 1990. As recommended by both the U.S. Environmental Protection Agency (U.S. EPA, 1984) and the California Air Resources Board (CARB, 1989), a formal protocol which outlined these evaluation techniques was submitted to the GBUAPCD prior to the initiation of study (TRC, 1991). Section 3 describes the model evaluation procedures proposed in the protocol that were employed in the study. Section 4 presents the results of the performance evaluation and Section 5 concludes the report with a summary of the study.

2.0 Model and Emission Factor Selection and Overview

The Mono Lake Evaluation Study investigated two dispersion models, the Industrial Source Complex Short-Term (ISCST) model (U.S. EPA, 1987a) and the Fugitive Dust Model (FDM) (Winges, 1990). ISCST is the U.S. EPA's currently recommended approach for regulatory assessments associated with fugitive dust (U.S. EPA, 1986a) and for air pathway analysis at superfund sites (U.S. EPA, 1989). ISCST is also the model preferred by the CARB for bounding calculations of ground level area sources of fine particles or gaseous pollutants (CARB, 1989). FDM has recently been developed and was specifically designed for computing concentrations and deposition fluxes from fugitive dust sources (Winges, 1990). The deposition algorithms within FDM include many of the routines suggested by the CARB for estimation of the deposition flux from particulate sources. An overview of these models and previous evaluation studies is provided below.

The prediction of wind-blown PM_{10} emissions from the playas surrounding Mono Lake was based on a series of tests conducted during the late summer of 1990 with a portable wind-tunnel erected over characteristic erodible surfaces. Although emission factors were available from the scientific literature, preliminary application of several of these techniques to conditions at Mono Lake were found to be unsatisfactory and inconsistent with visual evidence during historical dust events. The two emission factor relationships used in the present study were based on different interpretations of the data collected during the wind tunnel experiments.

2.1 ISCST Overview

The ISC models have historically been the regulatory preferred models for assessments involving stationary sources with special problems such as aerodynamic downwash, particle deposition, volume sources, and area sources. Both long-term (ISCLT) and short-term (ISCST) versions have commonly been applied. These models are based on the steady-state Gaussian plume formulation with modifications to allow for simulations of complex industrial sources in both rural and urban settings. Major features of these models are the special algorithms that have been included to simulate point sources subject to building wake effects. The vertical and horizontal dimensions of the Gaussian plume are specified by atmospheric stability class as functions of downwind distance. For rural conditions, conventional Pasquill-Gifford dispersion curves are applied, while for urban conditions the Briggs urban dispersion curves are utilized. Square area sources and volume sources are simulated using the virtual point source concept based on the initial dimensions of the source. Line sources must be simulated by a series of volume sources specified by the user in the model input file.

For fugitive dust problems, the ISC models are often applied because they include routines both to simulate area sources and to account for removal of mass at the surface caused by gravitational settling and dry deposition. In addition to prediction of ground level concentrations, the models can be applied to provide estimates of deposition flux, a requirement for some refined Superfund air pathway analyses. Gravitational settling is assumed to result in a tilted plume where the inclination is based on the ratio of the settling velocity to the wind speed. The lower boundary condition is treated by assuming partial reflection

at the surface. Partial reflection or removal at the surface is accounted for by reducing the strength of the image source using a reflection coefficient. The reflection coefficient is typically based solely on particle size and is not a function of the surface characteristics or meteorology. The functional form of the coefficient is primarily speculative and is not based on empirical or theoretical evidence (U.S. EPA, 1987a).

2.2 FDM Overview

FDM is based on an analytical solution to the advection-diffusion equation with gravitational settling, using gradient-transfer or K-theory and a deposition flux lower boundary condition. The deposition flux lower boundary condition is based on the deposition velocity concept where the deposition velocity is a function of particle size, surface roughness, and meteorological conditions. Although the model is based on K-theory, both vertical and horizontal eddy diffusivities are calculated from the more conventional Pasquill-Gifford dispersion curves. These dispersion curves can be adjusted to account for differing surface roughnesses and averaging times. For a non-depositing point source with appropriate surface roughness and averaging time assumptions, FDM will duplicate the concentration predictions of ISCST. Routines within FDM allow for the simulation of line, area, and point sources. Volume sources are not specifically treated by the model. FDM was designed specifically for fugitive dust assessments and does not contain algorithms for plume rise or building wake effects.

The incorporation of the function forms of the Pasquill-Gifford dispersion curves into the analytical solution to the advection-diffusion equation results in mass conservation problems. For large particles or high deposition fluxes, the effects can be significant at long downwind distances. FDM corrects the analytical solution to ensure mass consistency and in this respect offers an improvement over several other U.S. EPA nonguideline models which employ similar deposition algorithms.

FDM can simulate emissions from a rectangular area source with arbitrary orientation and in this regard is considerably more flexible and convenient than ISCST. This simulation is accomplished internally in FDM by dividing the area source into a series of line sources perpendicular to the wind direction, where the line source algorithm is similar to the routines employed by the U.S. EPA's CALINE3 model. The user can also exercise an option within the model, such that line sources are continually added until convergence of the area source algorithm is achieved. This latter option can be applied to obtain precise estimates for receptors at the edge or even within the area source.

2.3 Evaluation Studies

Five dispersion model evaluation studies have already been performed comparing ISCST and FDM. Three studies involved fugitive dust impacts associated with surface mining operations at both western and eastern mines. A fourth evaluation compared the two models to results of a dual tracer experiment conducted at Hanford in eastern Washington. In all of these four studies, FDM significantly outperformed ISCST (Winges, 1990). The most relevant previous dispersion model evaluation study involved a comparison of ISCST and FDM with observations of wind-blown dust at the Bunker Hill Superfund site near Kellogg,

Idaho (TRC, 1990). At the Bunker Hill Site, the focus of the air pathway investigation involved wind-blown dust from exposed area sources. Along with a theoretical comparison, both models were evaluated against ambient data collected during the summers of 1987 and 1988. While the authors of this study also recommended the application of FDM, the performance differences between the models were found to be much less than the uncertainties associated with the emission algorithms employed for wind-blown dust.

Although previous evaluation studies are relevant, the present study specifically evaluates FDM and ISCST performance with respect to wind-blown PM_{10} sources at Mono Lake. Site specific performance evaluations are usually recommended by the U.S. EPA (1986a) and the CARB (1989) whenever a nonguideline model is being considering for a potential regulatory application. In addition, previous studies focused primarily on total suspended particulates (TSP) and some of the differences between the models in these studies were attributed to the simulation of the coarse size fraction. The present study also evaluates two emission algorithms which were not used in previous studies.

2.4 Emission Factor Overview

Historical dust episodes at Mono Lake occurred more frequently during the spring when the surface crust of the playas were thin. During the more erodible periods of the year, the wind tunnel tests conducted at Mono Lake indicated that PM_{10} emissions were strong functions of wind speed when wind speeds were a threshold value of about 16 to 20 mph[1]. PM_{10} emissions were correlated to the horizontal flux of saltating sand size particles and PM_{10} emissions fell rapidly once the supply of the larger saltating particles in the tunnel test section were depleted (Cowherd, 1991a). Surface crusting was also found to influence the value of threshold wind velocity, with strong surface crusts often forming during the summer months reducing the potential for PM_{10} emissions.

The two emission factors investigated in the present study assumes that for actual conditions at Mono Lake, the supply of saltating particles would not be limited because of the supply of these particles from upwind source areas. Using the higher observed PM_{10} emission rate data obtained during the initial sampling period of the wind tunnel tests, Ono (1991) found that PM_{10} emissions followed an exponential relationship with wind speed:

$$q_a = 9.35 \cdot 10^{-6}\ e^{0.13 \cdot u} \qquad (1)$$

where q_a is the area source PM_{10} emission factor or vertical flux ($g/m^2/sec$) and u is wind speed (mph). Ono suggests that this equation applies for wind speeds above 16 mph, the lowest erosion threshold observed in the wind tunnel tests. For the purposes of the discussion, tables, and figures that follow in this report, the emission factor in Equation 1 will be referred to as the "GBUAPCD" wind-blown emissions algorithm.

---

[1]Wind velocities refer to a measurement height of 10 m.

As an alternative to the above expression, Cowherd (1991b) proposed an algorithm for wind-blown PM_{10} emissions at Mono Lake which followed a cubic wind speed dependency above a threshold velocity:

$$q_a = 7.1 \cdot 10^{-7} (u - u_t)^3 \quad (2)$$

where u_t is a threshold velocity (mph), u, and are q_a defined as in Equation 1. The cubic wind speed dependency is more consistent with the majority of the emission factor relationships for wind-blown dust found in the scientific literature and also provides a reasonable fit to the wind tunnel data. A wind speed threshold of 18 mph was used for the purposes of the present evaluations based on the approximate average value observed in the wind tunnel tests used by Cowherd. The area source emission factor predicted by Equation 2 will be referred to as the "MRI" algorithm in the discussion that follows.

A comparison of the wind speed dependencies of the emission factors is presented in Figure 2-1. The MRI routine predicts much lower PM_{10} emissions for wind speeds below 25 mph and higher emissions above the value. The wind tunnel tests were generally conducted over a wind speed range of 25 to 42 mph. The behavior of the PM_{10} emissions from the Mono Lake playas to relatively lower wind speeds could not be determined from the wind tunnel tests. It was anticipated that the model evaluation study would provide some indication of which emission routine provided a better description of wind-blown PM_{10} emissions at Mono Lake.

Emission Factor Wind Speed Dependency

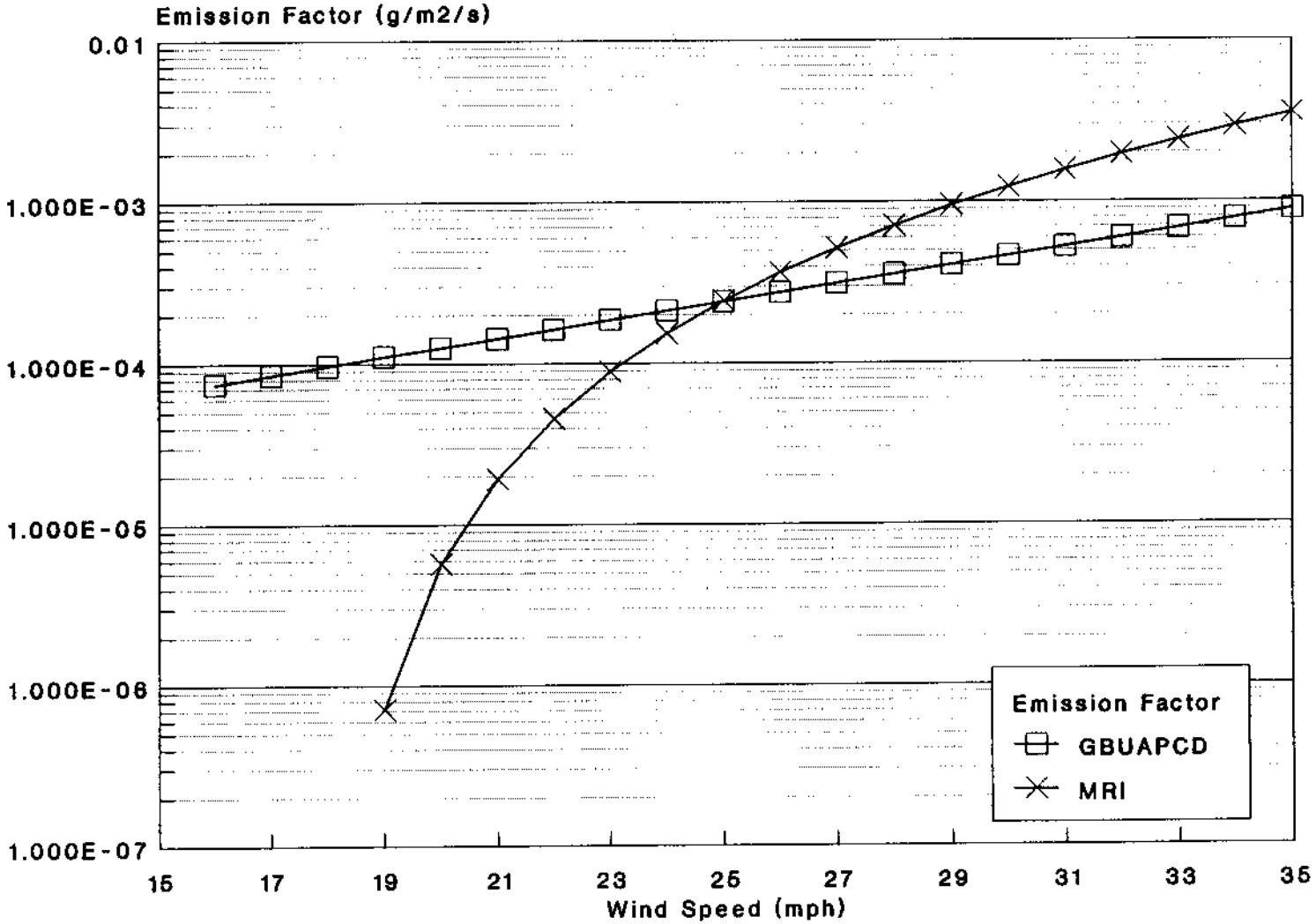

GBUAPCD - 9.35e-6*exp(.13*ws)
MRI - 7.1e-7*(ws-18)^3

Figure 2-1

3.0 Evaluation Methodology

The techniques used to evaluate the ISCST, FDM, and the two emission algorithms were based on the EPA's Interim Procedures for Evaluating Air Quality Models (U.S. EPA, 1984), on suggestions based on experience with the implementation of these procedures (U.S. EPA, 1985), and on the guidelines recommended by the CARB (1989). The analysis involved three steps: a technical comparison of the models, a series of sensitivity tests where the models were applied to representative wind-blown dust sources, and a performance evaluation which compared the models with ambient observations. For the performance evaluation, confidence limits and statistical measures in the analysis followed recent suggestions outlined by Cox (1987) and Hanna (1989).

3.1 Technical Comparison and Sensitivity Tests

The first step of the evaluation was a technical comparison of FDM with ISCST following the Workbook for Comparison of Air Quality Models (U.S. EPA, 1978). The procedure involved a subjective technical comparison of the components of the dispersion models with an emphasis on those algorithms more important or relevant to the objectives of the application. For the current study, the emphasis was on the routines controlling the dispersion, plume depletion, and deposition of wind-blown PM_{10} from area sources.

A sensitivity analysis was performed, where the model and emission routines were applied to a hypothetical area source under a variety of conditions. The purpose of these tests was to contrast the behavior of the models given the same set of input parameters, and to identify conditions under which the models function unreasonably. These tests also aided in the interpretation of the relative model differences that became apparent during the performance evaluation. The input parameters were varied systematically with a range of particle sizes, surface roughnesses, meteorological conditions, downwind receptor distances, and area source configurations.

3.2 Performance Evaluation

The next step in the overall assessment was the performance evaluation, where FDM, ISCST, and the two emission algorithms were compared to observations collected within Mono Basin. The primary objective of the performance evaluation was to determine which models more adequately described ambient PM_{10} observations during conditions conducive to wind-blown dust events. The remainder of this section presents the ambient data sets that were used in the analysis, a discussion of the statistical measures, and the methods used to prepare the input data necessary for model application.

3.2.1 PM_{10} Data Sets

The locations of the PM_{10} monitoring sites with respect to the exposed shores of Mono Lake are shown in Figure 3-1. The areas of visually observed wind-blown emissions are also outlined in this figure. In addition to PM_{10} samples, a meteorological station was also located at the Simis site which collected wind, temperature and precipitation data. Due to the nature of the prevailing winds, the Lee Vining site

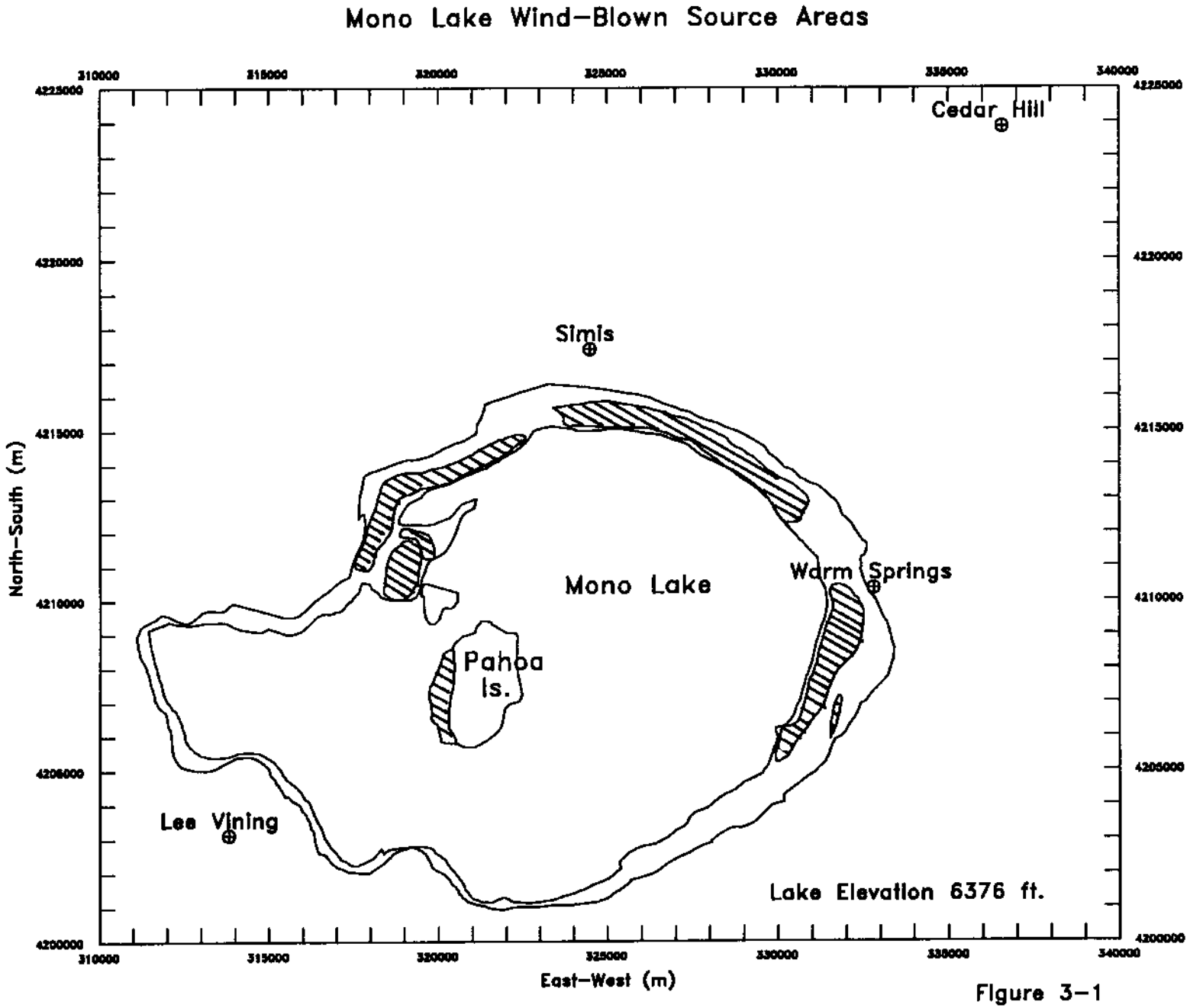
Mono Lake Wind-Blown Source Areas
310000
315000
320000
325000
330000
335000
340000
4225000
4220000
4215000
4210000
4205000
4200000
Cedar Hill
Simis
Mono Lake
Warm Springs
Paoha Is.
Lee Vining
Lake Elevation 6376 ft.
North-South (m)
East-West (m)

Figure 3-1

served as a background site. Prior to June 1989, the Simis and Lee Vining sites operated on a one in six day schedule. After this period, sampling at Simis was increased to five in six days for several months. However due to the remote nature of the site, this sampling frequency proved logistically impractical and the sampling routine was modified. Since October 1989, PM_{10} samples at Simis have been obtained for three consecutive days in six. In addition during periods of predicted high winds, three consecutive daily samples were also collected at Simis. The Cedar Hill and Warm Springs sites were added to supplement the monitoring program late in 1989. These stations were also operated based on a prognostic wind analysis.

In order to emphasize wind-blown dust sources, only those days where wind velocities exceeded the threshold for wind suspension were considered in the evaluation. Days with significant precipitation were also excluded from the analysis. Based on wind tunnel tests conducted by the GBUAPCD, a typical erosion threshold for the majority of the playas surrounding Mono Lake was about 16 to 20 mph. The available data for those days with winds exceeding 20 mph for at least one hour are shown in Table 3-1. Note, that not all the sampling periods covered a full 24 hours and that on only two days were data available for all four stations. Predictions from both dispersion models using both emission algorithms were compared with the observations for each station (excluding Lee Vining the background station) and for the data set as a whole.

3.2.2 Statistical Performance Measures

Several different statistical performance measures were employed during the reconciliation of the ISCST, FDM, and emission models with observations. The measures were selected to evaluate the abilities of the models to :

- explain the mean and standard deviation of the observations
- explain the higher values of the observations
- explain the temporal and spatial variation of the observations

In order to test whether the dispersion models can explain the frequency distribution of the observations, Cox (1987) suggested that the fractional bias of the average and of the standard deviation be employed. The fractional bias of the mean (F_b) and of the standard deviation (F_σ) are given by:

$$F_b = 2\,\frac{(\overline{O} - \overline{P})}{(\overline{O} + \overline{P})} \tag{3}$$

$$F_\sigma = 2\,\frac{(\sigma_o - \sigma_p)}{(\sigma_o + \sigma_p)} \tag{4}$$

Table 3-1. PM-10 Episode Days
With Wind Speeds above 20 MPH

Date	PM10 (ug/m3) Simis	Warm Springs	Lee Vining	Cedar Hill
05/04/88	26 *	64 *		
05/15/88	14		7	
05/16/88		405 *		
09/19/88	34			
10/13/88	12			
11/06/88	71			
04/21/89	450 *		30 *	
05/28/89	24		5	
06/15/89	21		15	
10/20/89	25			
10/24/89	68			19
01/12/90	69			6
03/10/90	55			50
05/21/90	15	81 *		11
05/23/90	78	306 *	17	35
09/14/90	16		9	21 *
10/30/90	25			9
10/31/90	43	9 *		16
11/13/90	73	19 *	8	3
11/25/90	120		24	
04/30/91	72	201 *	21	20
05/08/91	75	389		
05/16/91	100	587 *		26
No. Samples	22	9	9	11

(*) denotes a sample of less than 24 hours or during a period other than a calendar day.

where "o" refers to the observations and "p" refers to the model prediction. The fractional bias has the advantage of being a symmetrical and bounded measure and because it's normalized it can be used for comparing results from studies involving different dependent variables. Values of the fractional bias vary from -2 (extreme over-prediction) to 2 (extreme under-prediction). Predictions within a factor-of-two are bounded by a fractional bias of ± 0.667.

The statistical measures above emphasize the model's abilities to predict the whole domain of the observations. In order to focus on the higher observations, the fractional bias of the "robust highest concentration" (F_{RHC}) was also calculated. After Cox, the RHC was based on the following:

$$RHC = X_n + (\overline{X_N} - X_n) \ln\left(\frac{3n-1}{2}\right) \quad (5)$$

where X_n was the nth highest value

$\overline{X_N}$ was the average of the n-1 highest values

n was the number of high values

The value of n is somewhat arbitrary but is typically chosen to be 26 or the number of concentrations exceeding a threshold value. For the purposes of the present analyses, n was selected as 10, roughly the number of times that PM_{10} observations at Simis exceeded the CAAQS. In addition due to a limited number of samples at Cedar Hill and Warm Springs, RHC's were not calculated for these individual data sets.

When applied to the data sets given in Table 3-1, the performance measures listed above do not require that the models explain the temporal and spatial distribution of the observations. While this may be adequate for many regulatory applications, more rigorous statistical tests involve statistical measures which are paired in time and space. In the performance evaluation, the normalized mean square error (NMSE) and the linear correlation coefficient (r) between model predictions and observations were also determined from the following:

$$NMSE = \frac{\overline{(O - P)^2}}{\overline{O}\,\overline{P}} \quad (6)$$

$$r = \frac{\frac{1}{N}\sum_{i=1}^{N}(P_i - \overline{P})(O_i - \overline{O})}{\sqrt{\left(\frac{1}{N}\sum_{i=1}^{N}(P_i - \overline{P})^2\right)\left(\frac{1}{N}\sum_{i=1}^{N}(O_i - \overline{O})^2\right)}} \quad (7)$$

Both of these measures test the scatter of model predictions about the observations. If the NMSE equals 1.0, then the typical difference between predictions and model observations is approximately equal to the mean. The linear correlation coefficient is a less rigorous test than the NMSE, because a high correlation coefficient can be still be obtained when the bias (intercept) or the scale (slope) of the model predictions are different than zero and one, respectively. However, the correlation coefficient is less sensitive to assumptions regarding background concentration.

The statistical significance of differences between the performance measures calculated for each model depend on the characteristics of the data sets and on sample size. In order to assess the statistical uncertainty involved in the calculation of each performance measure and to assess whether the differences found were significant, confidence limits were estimated. Confidence limits were based on the moment bootstrap method (Hanna, 1989), where the bootstrap or resampling was used to estimate the uncertainty in the performance measure. Given a data set containing N values, the resampling process involved repetitively selecting N values at random from the original data set. For each resampled set, a new performance measure was calculated. In the moment bootstrap method, the resampling is used only to determine the mean and the variance of the distribution of the performance measure. Confidence limits were based on the Student's-t procedure. For example, the 95% confidence limits of the NMSE were:

$$\overline{NMSE} - t_{95}\sigma_{NMSE} < x < \overline{NMSE} + t_{95}\sigma_{NMSE} \qquad (8)$$

where t_{95} was based on the Student's-t distribution with (N-1) degrees of freedom. The mean and standard deviation of each performance measure used in the relative comparison were determined by randomly resampling each of the data sets many times. A value of 200 repetitions was determined by trial and error as the number required to achieve stable results. Using different values of the Student's-t distribution, 95%, 90%, and 80% confidence limits were calculated for each performance measure.

3.2.3 Input Data Preparation

This section describes the manner in which input data were prepared in the Mono Lake Evaluation Study. The required input data for each model include an emission inventory, a meteorological data set, and background concentration estimates. The techniques used to estimate wind-blown emissions from the exposed shores of Mono Lake vary hourly with wind speed according to Equations 1 & 2 in Section 2-4. The source codes of both dispersion models were modified so that they could accept an hourly variable emissions specified in an external data file.

Figure 3-2 presents an hourly time series plot of the GBUAPCD and MRI emission factor predictions for the episode days considered in the study. As expected the MRI cubic relationship tended to produce the higher peak hourly values, 0.00185 versus 0.00058 $g/m^2/sec$ for the GBUAPCD method. However for many of the PM_{10} sampling periods wind speeds in the range of 16 to 25 mph were prevalent and for these days the GBUAPCD algorithm yielded the higher wind-blown PM_{10} emission fluxes. Average PM_{10} emission

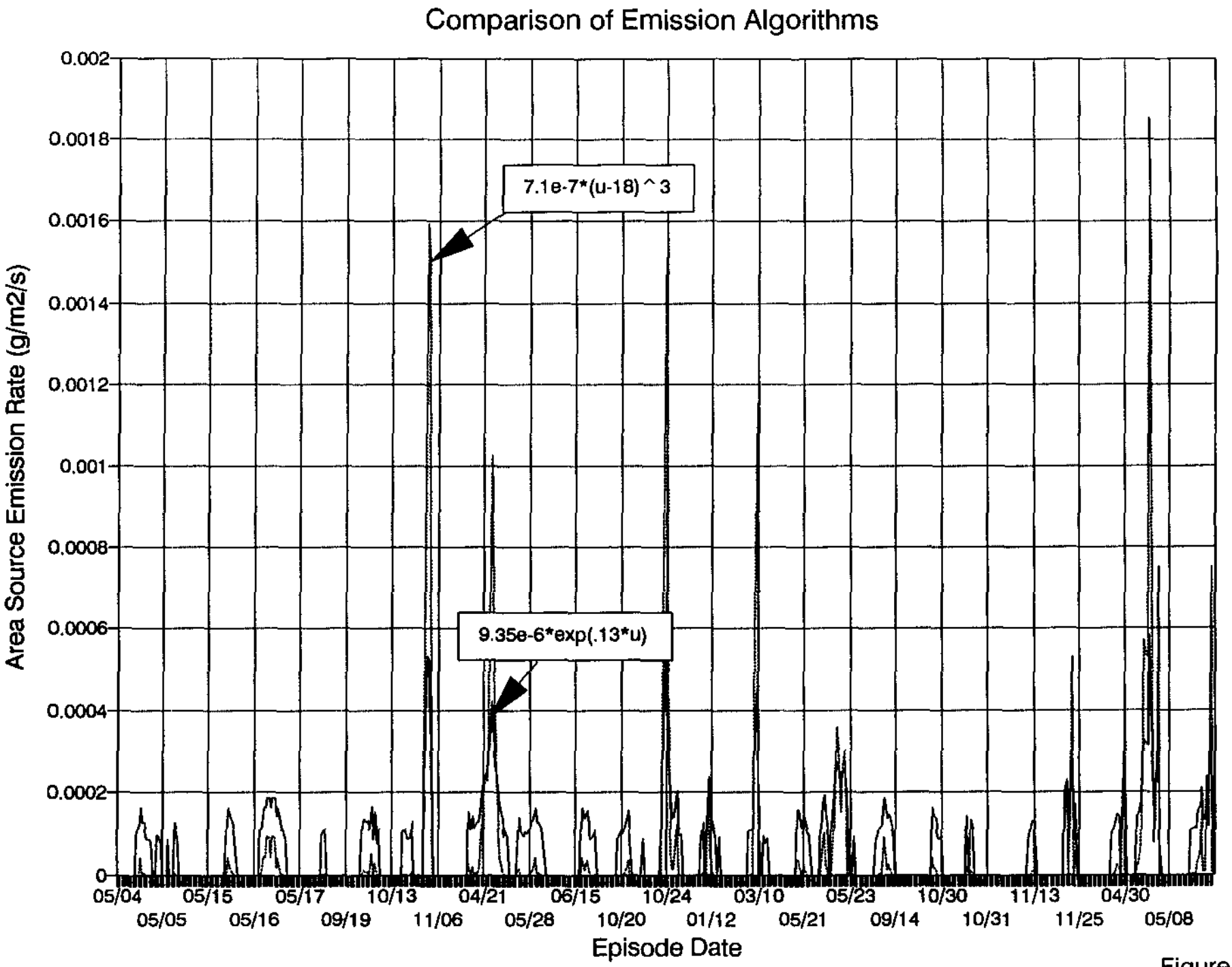
Comparison of Emission Algorithms
Area Source Emission Rate (g/m2/s)
0.002
0.0018
0.0016
0.0014
0.0012
0.001
0.0008
0.0006
0.0004
0.0002
0
7.1e-7*(u-18) ^ 3
9.35e-6*exp(.13*u)
05/04
05/05
05/15
05/16
05/17
09/19
10/13
11/06
04/21
05/28
06/15
10/20
10/24
01/12
03/10
05/21
05/23
09/14
10/30
10/31
11/13
11/25
04/30
05/08
Episode Date

Figure 3-2

factors for the 22 sampling days were $4.53 \cdot 10^{-5}$ and $6.23 \cdot 10^{-5}$ $g/m^2/sec$ for the MRI and GBUAPCD techniques, respectively.

FDM and ISCST are based on a cartesian coordinate system where winds are assumed to be spatially uniform throughout the modeling region. Area sources in FDM must be specified as rectangles, and are further restricted to be squares which are aligned in the east-west direction by ISCST. In order to prepare the model emission input files, the estimates provided by MRI/GBUAPCD were mapped on to a series of rectangular area sources which roughly correspond to the irregular source areas outlined in Figure 3-1. Figure 3-3 displays the area source configuration used in the FDM simulations. Beyond the definition of specific source areas, neither the GBUAPCD or MRI emission factor methods account for any spatial variation in emissions and estimates for any given wind speed were the same for all the source areas defined in Figure 3-3.

The area source configuration used in the ISCST simulations is presented in Figure 3-4. For ISCST, the area sources were further broken down into a number of smaller squares, such that the side of the largest square was smaller than downwind distance to the nearest receptor. This was necessary due to the close proximity of the Warms Springs station to the playas on the eastern shore of Mono Lake. The application ISCST to the Mono Lake area sources required the simulation of many more individual square area sources than were necessary for FDM.

In addition to the specification of emission rates and area source configuration, both FDM and ISCST require airborne particle size distribution information which influences the deposition and plume depletion predictions. For the simulation of PM_{10} sources, assumptions concerning the airborne particle size distribution are less important than for predictions involving coarser particles and depletion of PM_{10} from the plume due to interactions with the surface is often conservatively neglected. However, for low level sources the depletion of mass even for the relatively fine particles can be significant for long travel times (See Appendix B).

In the absence of data collected on site, model simulations were based on an airborne particle size distribution taken from the literature. During wind-blown dust events the majority of the suspended mass is contained in particles larger than 10 μm, with a median diameter typically near 50 μm (Pye, 1987). For particles within the PM_{10} size range, Gillette reports that during wind-blown dust events the number of particles per logarithmic interval can be described by a function which decreases with the square of particle diameter (Gillette et. al., 1974). This functional form indicates that particle mass per logarithmic interval would increase linearly with particle diameter as shown in Table 3-2. Both ISCST and FDM model simulations were performed with the distribution given in Table 3-2. Several sensitivity tests with different particle size distributions indicated that for the relatively close critical receptors in the current study, particle size assumptions did not overly influence the model simulations. Further discussion concerning particle size distribution sensitivity is presented in Appendix B.

Table 3-2. PM-10 Particle Size Distribution

Diameter Range(um)	Mean Diameter(um)	Mass Fraction
0.10 - 0.25	0.16	0.015
0.25 - 0.63	0.40	0.039
0.63 - 1.60	1.00	0.096
1.60 - 3.98	2.51	0.242
3.98 - 10.0	6.31	0.608

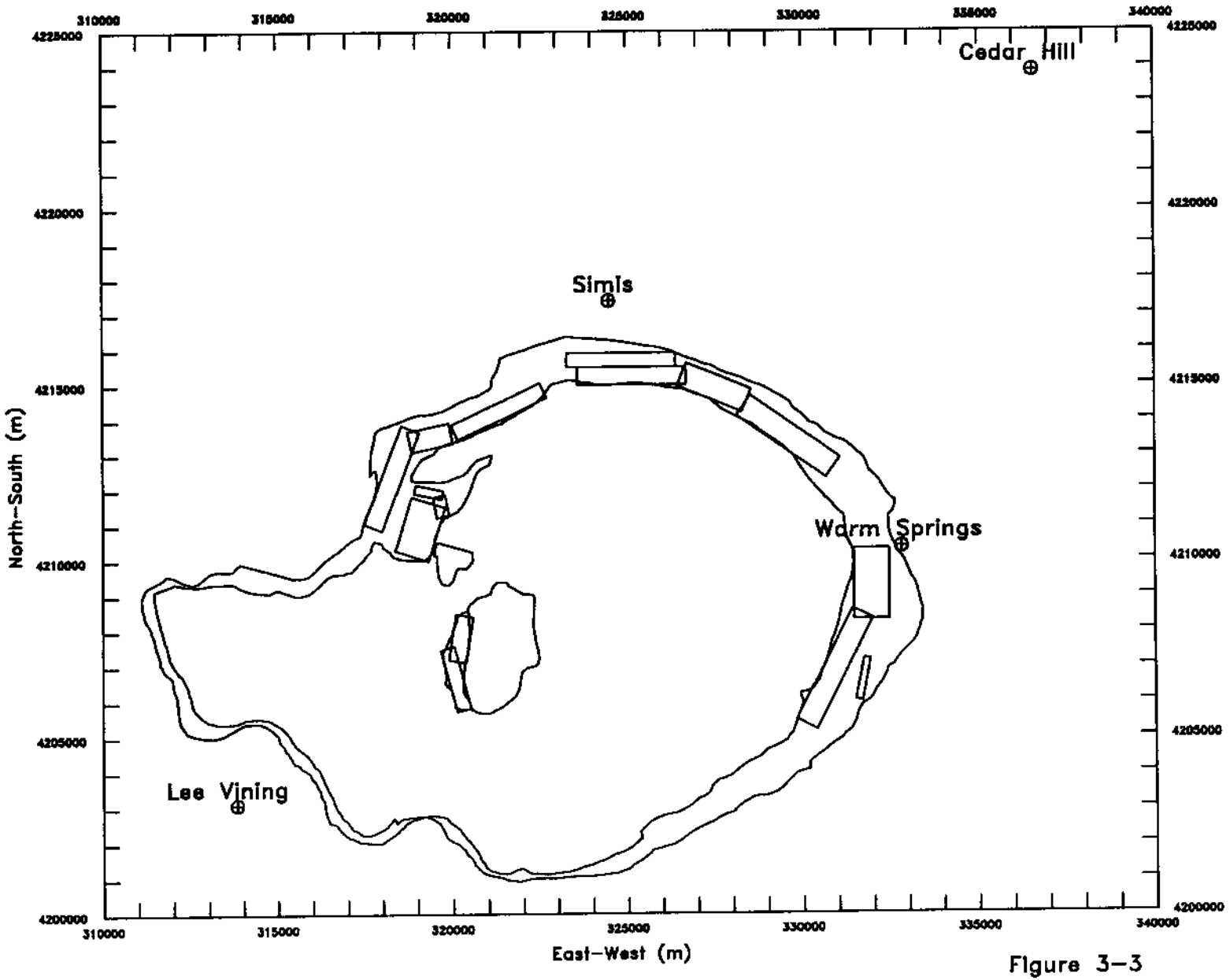
FDM Area Source Configuration
Cedar Hill
Simis
Warm Springs
Lee Vining
North-South (m)
East-West (m)
310000
315000
320000
325000
330000
335000
340000
4225000
4220000
4215000
4210000
4205000
4200000

Figure 3-3

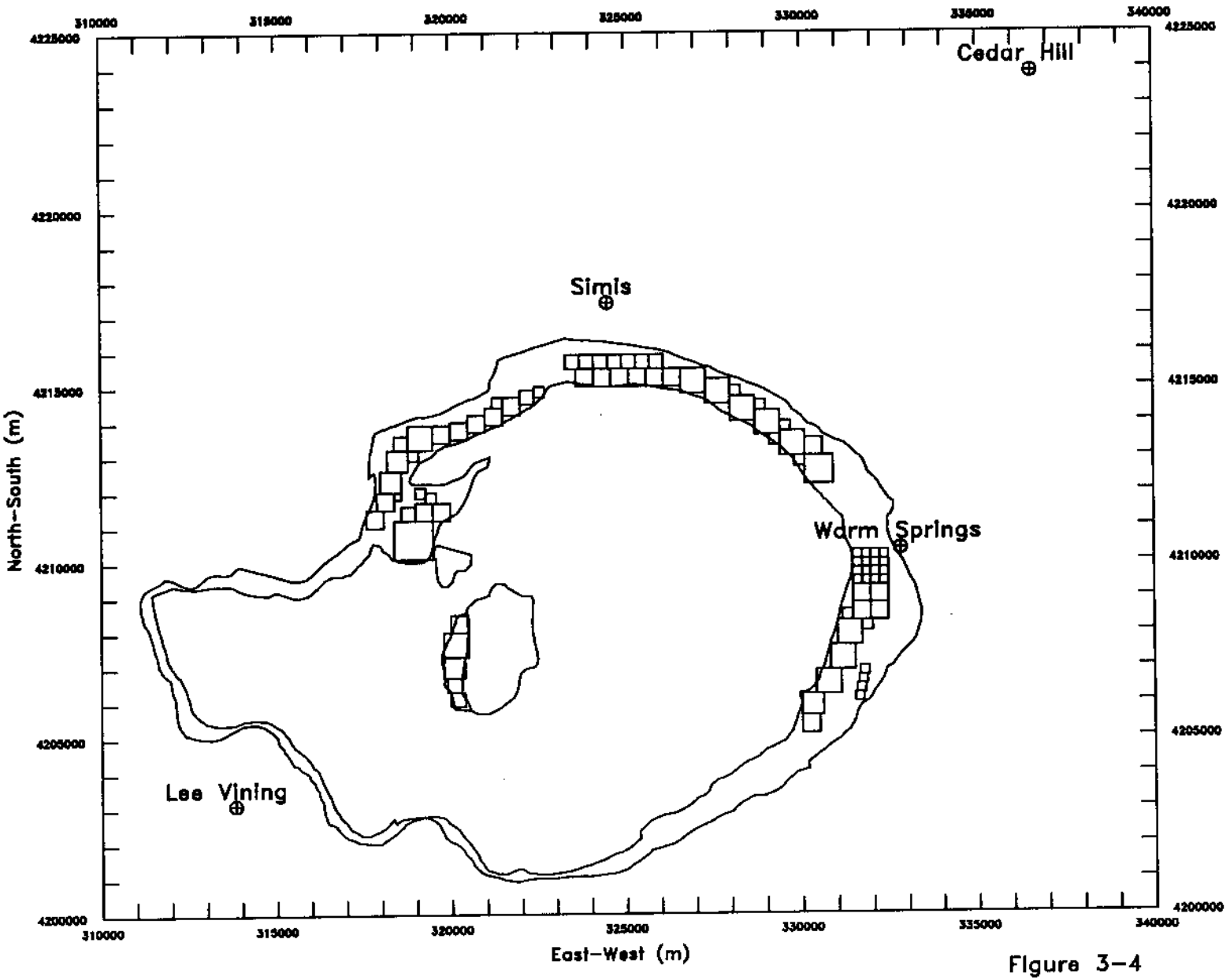
ISC Area Source Configuration
Cedar Hill
Simis
Warm Springs
Lee Vining
North-South (m)
East-West (m)
310000
315000
320000
325000
330000
335000
340000
4225000
4220000
4215000
4210000
4205000
4200000

Figure 3-4

Hourly meteorological data files were constructed using the observations from the Simis site during 1988 to 1991. The data set included only those PM_{10} sampling periods where at least one hour of wind speed was observed to exceed 20 mph and those days when significant precipitation was absent. A wind rose constructed from the data set is shown in Figure 3-5. These data indicated that the majority of the relatively high winds in the data set were from the south to west-southwest. Average wind speeds for these directions were 7.4 m/s (16.5 mph) near the threshold of wind suspension found in the wind-tunnel tests.

In addition to the wind speed, wind direction, and temperature observations, both dispersion models require hourly estimates of atmospheric stability class and the depth of the well mixed layer. Atmospheric stability class estimates were based on wind speed, sigma-theta, and the time of day according to the guidelines specified by the U.S. EPA (1987b). In order to be consistent with the practices followed by both the U.S. EPA's RAMMET and MPRM meteorological data pre-processor programs, the hourly stability class estimates were smoothed prior to input into the dispersion models by not allowing stability to change by more than one class per hour. The definition of day and night used by the EPA's regulatory pre-processor program was also followed.

Hourly mixing height data were based on the twice daily climatic average values given by Holzworth (1972). Values interpolated from this reference are shown in Table 3-3. Hourly values were estimated from the average morning and afternoon mixing height using the interpolation routines employed by both the U.S. EPA's MPRM and RAMMET meteorological pre-processors. The mixing height information was used by both ISCST and FDM to simulate plume trapping beneath a strong subsidence inversion. In order to ensure that low mixing heights do not occur during windy conditions, the hourly mixing heights were not allowed to be less than a estimated minimum mechanical mixing depth of 100m (U.S. EPA, 1986b). For the simulations at Mono Basin, the vertical depth of the dust plumes at the receptors most impacted were less than the depth of the mixed layer and plume trapping was not important.

The dispersion model simulations only included wind-blown sources of PM_{10} from the exposed shores of Mono Lake. During high wind events other local and regional sources of fugitive dust could also contribute to the PM_{10} levels observed at the monitoring locations. In order to estimate background PM_{10} levels, the data from the Lee Vining site was used. Examination of Figures 3-1 and 3-5 indicates that during periods of high wind velocity Lee Vining was upwind of the dust source areas and the other monitoring stations. When data from this station was unavailable for a given sampling period, the background PM_{10} concentration was based on the overall average of the Lee Vining PM_{10} data in Table 3-1. The average observed Lee Vining PM_{10} concentration was 15 $\mu g/m^3$.

The final meteorological parameter required in the dispersion modeling simulations was the surface roughness length. In FDM this parameter influences both the dispersion and deposition routines, such that a large surface roughness results in increased dispersion and higher deposition velocities. Field experiments which have collected turbulence data indicate that during high wind or neutral conditions, sigma-theta data

Table 3-3. Holzworth Seasonal Mixing Heights

Season	Mean Morning Mixing Ht(m)	Afternoon Max Mixing Ht(m)
Winter	400	1000
Spring	650	2500
Summer	300	3000
Autumn	350	2000

Mono Lake Evaluation Study
Days with PM10 Data & Winds > 20 mph

DATA PERIOD - MAY 4, 1988 THROUGH MAY 16, 1991
MONTHS CONSIDERED - JAN THROUGH DEC
HOURS CONSIDERED - 0 TO 2400

WIND FREQUENCY DISTRIBUTION
FREQUENCY IN PERCENT
OF TOTAL OBSERVATIONS

	WIND SPEED CLASS (MPS)									
WIND SECTOR	.51 TO 1.50	1.51 TO 3.00	3.01 TO 5.00	5.01 TO 7.50	7.51 TO 10.00	10.01 TO 15.00	15.01 TO 20.00	GREATER THAN 20.00	TOTAL	MEAN SPEED
NNE	2.00	3.00	.67	.50	.33	.00	.00	.00	6.50	2.64
NE	2.17	2.17	1.33	.00	.00	.00	.00	.00	5.67	2.19
ENE	1.67	.83	.67	.00	.00	.00	.00	.00	3.17	1.83
E	.67	1.00	.50	.00	.00	.00	.00	.00	2.17	2.13
ESE	.33	.33	.33	.00	.00	.00	.00	.00	1.00	2.30
SE	.33	.17	.67	.00	.00	.00	.00	.00	1.17	3.19
SSE	.17	.33	.67	1.33	1.00	.00	.00	.00	3.50	5.90
S	1.33	1.67	1.67	3.00	8.00	3.00	.00	.00	18.67	7.17
SSW	1.83	.67	1.83	4.33	9.17	3.17	.00	.00	21.00	7.31
SW	.17	.67	1.67	2.67	4.17	1.67	.00	.00	11.00	7.30
WSW	.17	.83	.83	1.33	3.67	1.83	.00	.00	8.67	7.79
W	.17	.17	1.00	.83	1.00	.33	.00	.00	3.50	6.65
WNW	.50	.50	.67	.50	.33	.00	.00	.00	2.50	3.91
NW	.67	.17	.83	.33	.00	.00	.00	.00	2.00	3.33
NNW	1.17	2.00	.67	.17	.00	.00	.00	.00	4.00	2.42
N	2.17	1.83	.67	.17	.17	.00	.00	.00	5.00	2.33
CALM									.50	
TOTAL	15.50	16.33	14.67	15.17	27.83	10.00	.00	.00	100.00	5.63

NUMBERS BELOW BASED ON ALL OBSERVATIONS
NUMBER OF INVALID OBSERVATIONS = 0
NUMBER OF VALID OBSERVATIONS = 600

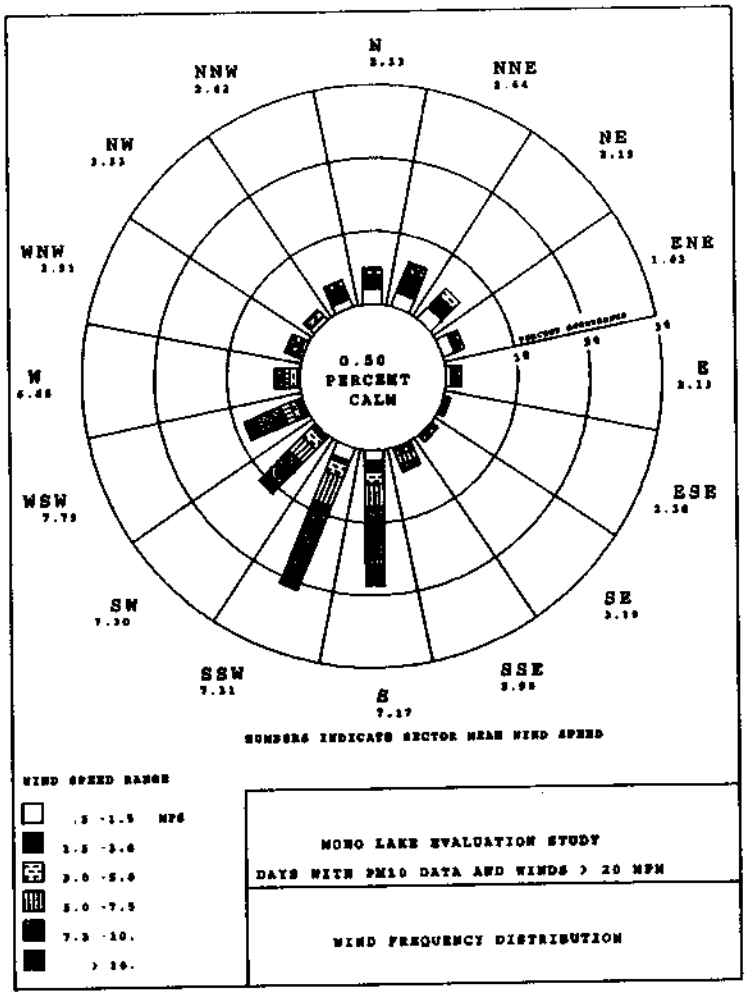

Figure 3-5

approach a constant value depending on the effective upwind roughness (Arya, 1988). The effective surface roughness is a function of the scale of the upwind terrain features in addition to the local characteristics of the upwind surfaces.

Figure 3-6 displays a plot of sigma-theta versus wind speed for the Simis station which indicates a trend toward a constant value for the hourly average sigma-theta data of about 10 degrees for high wind speeds. An effective surface roughness length was estimated from the sigma-theta data during high wind conditions based on:

$$z_o = z_{ref} e^{-2\frac{k}{\sigma_\theta}} \tag{9}$$

where σ_θ is the 10 minute average sigma-theta (radians) value during high wind conditions, k is von Karman's constant taken to be 0.4, z_o is the roughness length (cm), and z_{ref} is the height of the anemometer (1000 cm). Ten minute sigma-theta data were estimated from the 60 minute average data collected at Simis using a power law (Turner, 1970). Using these assumptions, the effective roughness length was plotted against wind speed in Figure 3-6 and found to trend toward a value of 1 cm which was used in the FDM model simulations. The sensitivity of the FDM simulations to surface roughness assumptions are provided in Appendix B.

Roughness Length For Winds Above Indicated Threshold at Simis

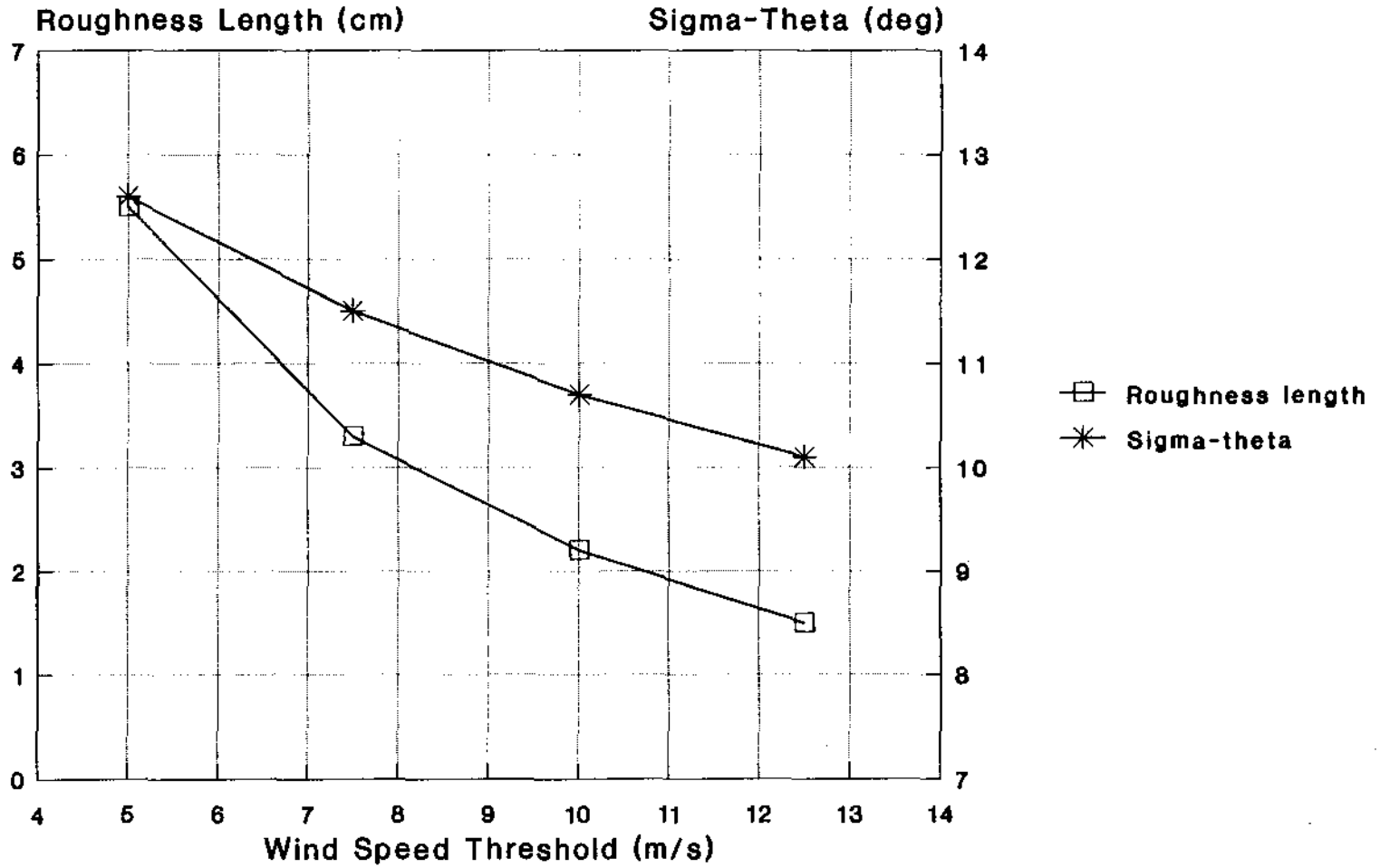

Episode days with PM10 data

60-minute sigma-theta data

Figure 3-6

4.0 Model Evaluation Results

The objective of the Mono Lake Evaluation Study was to assess dispersion modeling techniques for the prediction of PM_{10} concentrations during high wind events. The study included the evaluation of FDM and ISCST and two alternative methods for the estimation of wind-blown PM_{10} emissions. The model evaluation involved three steps: a technical comparison of the models, a series of sensitivity tests where the models were applied to representative wind-blown dust sources, and a performance evaluation which compared the models and alternative emission factors with ambient observations. The methods used in the evaluation including the selection of PM_{10} data sets, input data preparation, estimation of confidence limits, and the statistical measures employed were discussed previously in Section 3. The results of the evaluation follow.

4.1 Technical Comparison and Sensitivity Tests

The results of the technical comparison are fully described in Appendix A. In summary, a technical comparison based on U.S. EPA guidelines for the use of nonguideline models indicated that FDM was better in three of the four possible application elements judged to be of high importance for simulations of wind-blown PM_{10} emissions from area sources at Mono Lake. The primary basis of this evaluation was that FDM's area source algorithm was more convenient to apply, and offers more consistency and greater precision for receptors close to large area sources. The manner in which an area source was configured influences both the horizontal and vertical dispersion parameters used by ISCST in an arbitrary way. Although less important to the application at Mono Lake, the physical removal mechanisms employed by FDM were also found to be better than those included in ISCST. Dry deposition, gravitational settling, and plume depletion tend to be more important for the simulation of particles larger than the PM_{10} size range, but could still influence model predictions at receptors sufficiently far downwind.

Appendix B presented the results of a sensitivity analysis which contrasted the behavior of the ISCST and FDM models to conditions representative of wind-blown PM_{10} emissions from the exposed shores of Mono Lake. For windy conditions and PM_{10} particles, the models were found to predict concentrations that were similar to one another. However, some of this agreement was fortuitous and was attributed to the manner in which the area sources used in the ISCST tests were configured. The area source routine employed by the ISCST model was found to produce arbitrary results close to a large area source that depended on the degree of resolution used to divide the area source, the proximity of the receptor, and wind direction. Among the other parameters investigated, particle size was also found to influence the model predictions with FDM predicting a greater degree of plume depletion than the ISCST model. However due to the relative fine nature of PM_{10} particles, the differences between the models were relatively small for distances less than about 10 km.

4.2 Performance Evaluation

The final step in the overall assessment was the performance evaluation, where FDM, ISCST, the MRI emission algorithm, and the GBUAPCD emission algorithm were compared to PM_{10} observations

collected within Mono Basin. Each model was applied to an hourly emissions data set following the two emission methods, then statistically compared with the PM_{10} data from the Simis, Cedar Hill, and Warm Springs monitoring stations. A background value of 15 $\mu g/m^3$ or when available the data from the Lee Vining station were added to the model predictions to account for upwind PM_{10} sources not included in the emissions inventory. Appendix C contains a full listing of the predictions from the four possible model/emission factor pairings with observations at the three stations. Note, that in some instances the sampling data and model predictions correspond to periods less than 24 hours.

Figure 4-1 presents the results of the model simulations with scatter diagrams of the four model/emission factor pairings with the ambient PM_{10} data. Although considerable scatter was evident, both the emission factors and models tended to significantly correlate with the ambient PM_{10} data. For all stations combined, linear correlation coefficients ranged from a high of 0.836 for the simulations based on FDM and the GBUAPCD emission factor, to 0.717 for the ISCST model simulating the MRI based emissions. The correlations of ISCST and FDM with ambient data were similar, however the GBUAPCD emission method produced less scatter than the MRI technique. As shown in Figure 4-1, the relatively lower correlation of the MRI based emissions can be attributed to the poor performance of this method for two of the episodes at Warm Springs. Both of these episodes had wind speeds less than 26 mph, in the wind speed range where the MRI emission routine predicts lower values than the GBUAPCD method (see Figure 2-1).

In order to test whether the dispersion models could explain the frequency distribution of the observations, values of the fractional bias of the average and of the standard deviation were calculated as suggested by Cox (1987). As a screening test for model performance, Cox proposed that fractional bias should be bounded by a value of ± 0.667 which represents a factor-of-two difference between model predictions and observations. A negative fractional bias implies overprediction. Figure 4-2 displays the results of the Cox screening test for the four possible model/emission factor pairings. Both models simulating emissions predicted by either the MRI or GBUAPCD routines pass the Cox screening test and were able to predict the mean and standard deviations of the observations within a factor-of-two.

Table 4-1 provides a summary of the performance statistics for the evaluation study. In addition to the fractional bias of the mean and standard deviation, the fractional bias of the Robust Highest Concentration (RHC) was also calculated to emphasize the models' ability to predict the relatively higher PM_{10} concentrations. Table 4-1 also includes the more rigorous statistical measures which were paired in time and space, the linear correlation coefficients and the NMSE. With the exception of the RHC, all the statistical performance measures were calculated for each station and for the data set as a whole. RHC's were not calculated for the Warm Springs and Cedar Hill individual data sets due to their relative small sample sizes.

Table 4-1. Model Performance Statistics

Data Set	Model	Emission Factor	PM10 Mean (ug/m3) Obs.	Pred	F_bias	PM10 Std Dev. (ug/m3) Obs.	Pred	F_bias	PM10 RHC (ug/m3) Obs.	Pred	F_bias	NMSE	Linear Corr. Coef.
All Stations Combined 42 samples	FDM	GBUAPCD	90	116	-0.259	135	128	0.051	654	581	0.118	0.604	0.836
	ISCST	GBUAPCD		103	-0.136		104	0.256		503	0.260	0.611	0.835
	FDM	MRI		77	0.152		139	-0.030		601	0.085	1.512	0.721
	ISCST	MRI		69	0.260		114	0.165		497	0.272	1.518	0.717
Simis Station 22 samples	FDM	GBUAPCD	68	103	-0.414	91	67	0.307	215	273	-0.237	0.659	0.760
	ISCST	GBUAPCD		96	-0.347		64	0.350		253	-0.162	0.629	0.767
	FDM	MRI		67	0.009		90	0.011		333	-0.429	0.571	0.834
	ISCST	MRI		64	0.049		86	0.055		320	-0.389	0.572	0.835
Cedar Hill Station 11 samples	FDM	GBUAPCD	20	29	-0.399	14	14	0.003	RHC not reported due the small sample size			0.399	0.606
	ISCST	GBUAPCD		31	-0.434		14	-0.057				0.455	0.571
	FDM	MRI		24	-0.218		16	-0.128				0.311	0.683
	ISCST	MRI		25	-0.257		17	-0.243				0.403	0.644
Warm Springs Station 9 samples	FDM	GBUAPCD	229	255	-0.106	204	200	0.019	RHC not reported due the small sample size			0.306	0.764
	ISCST	GBUAPCD		207	0.099		159	0.247				0.336	0.763
	FDM	MRI		166	0.321		254	-0.220				1.111	0.611
	ISCST	MRI		133	0.528		200	0.021				1.226	0.610

Note: RHC based on top 10 samples
GBUAPCD emissions from Qa(g/m2/s) = 9.35e-6*exp(.13*ws(mph))
MRI emissions from Qa(g/m2/s) = 7.1e-7*(ws(mph)-18) ^ 3
Negative bias implies overprediction

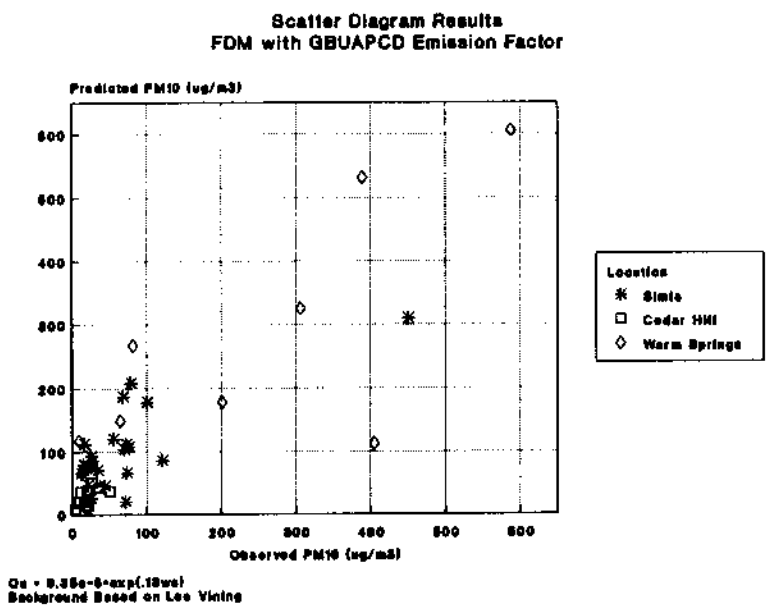
Scatter Diagram Results
FDM with GBUAPCD Emission Factor
Predicted PM10 (ug/m3)
Observed PM10 (ug/m3)
Location
Simis
Cedar Hill
Warm Springs
Qa = 9.38e-6*exp(.13ws)
Background Based on Lee Vining

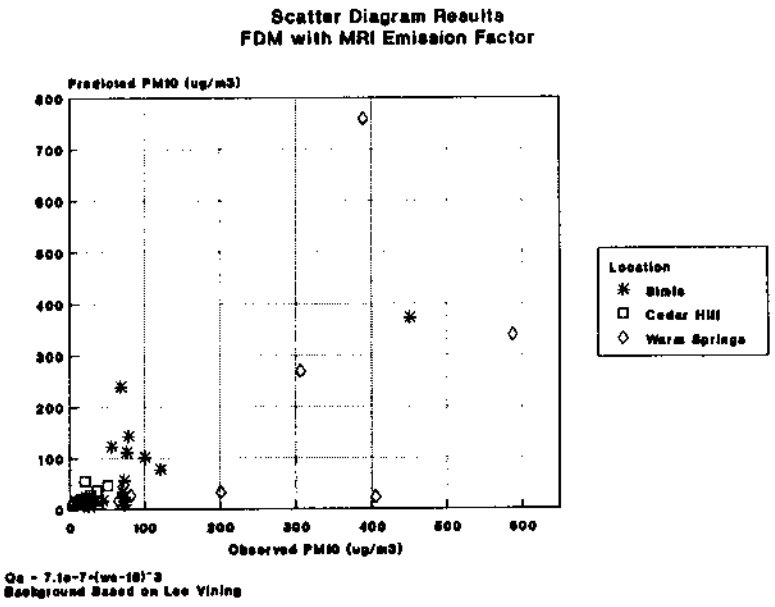
Scatter Diagram Results
FDM with MRI Emission Factor
Predicted PM10 (ug/m3)
Observed PM10 (ug/m3)
Location
Simis
Cedar Hill
Warm Springs
Qa = 7.1e-7*(ws-18)^3
Background Based on Lee Vining

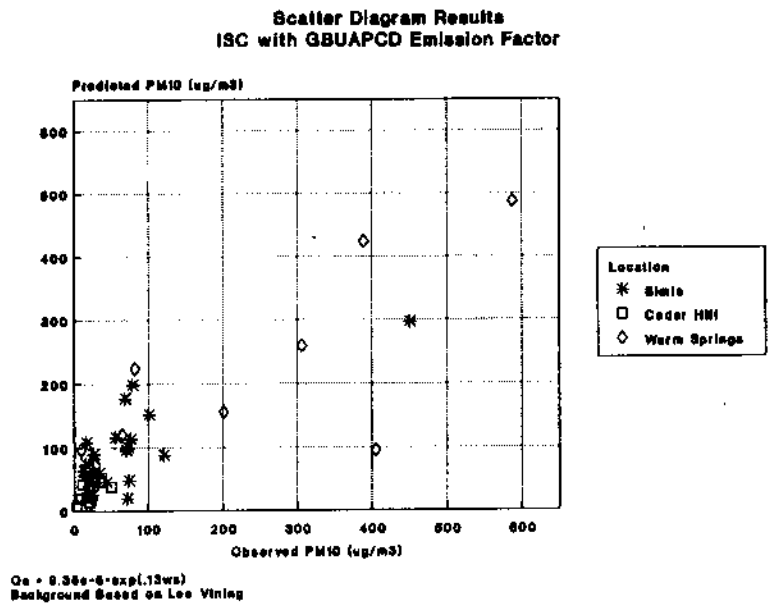
Scatter Diagram Results
ISC with GBUAPCD Emission Factor
Predicted PM10 (ug/m3)
Observed PM10 (ug/m3)
Location
Simis
Cedar Hill
Warm Springs
Qa = 9.38e-6*exp(.13ws)
Background Based on Lee Vining

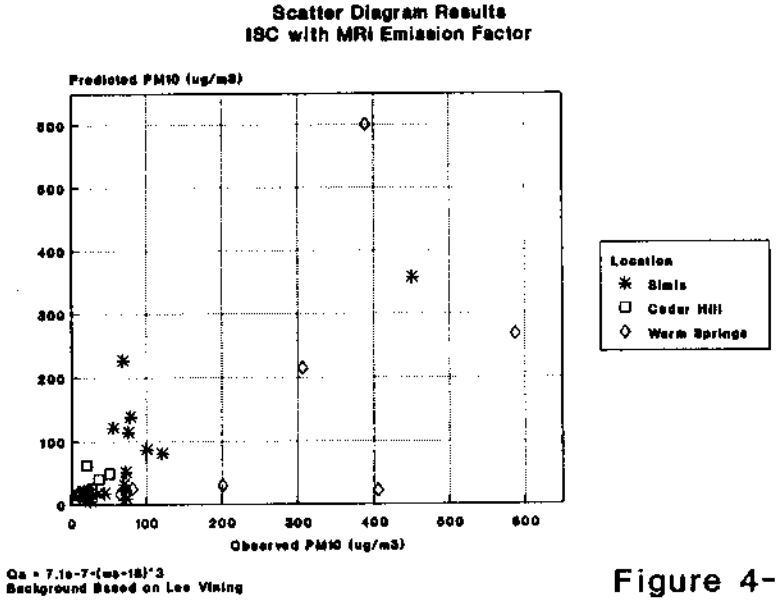
Scatter Diagram Results
ISC with MRI Emission Factor
Predicted PM10 (ug/m3)
Observed PM10 (ug/m3)
Location
Simis
Cedar Hill
Warm Springs
Qa = 7.1e-7*(ws-18)^3
Background Based on Lee Vining

Figure 4-1

Cox Screening Test Results
FDM with GBUAPCD Emission Factor

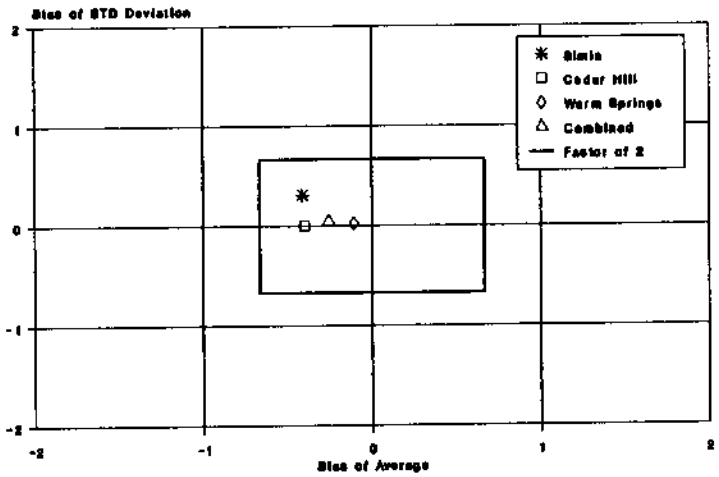

Qs = 9.36e-6*exp(.13ws)
Background Based on Lee Vining
Negative Bias Implies Overprediction

Cox Screening Test Results
FDM with MRI Emission Factor

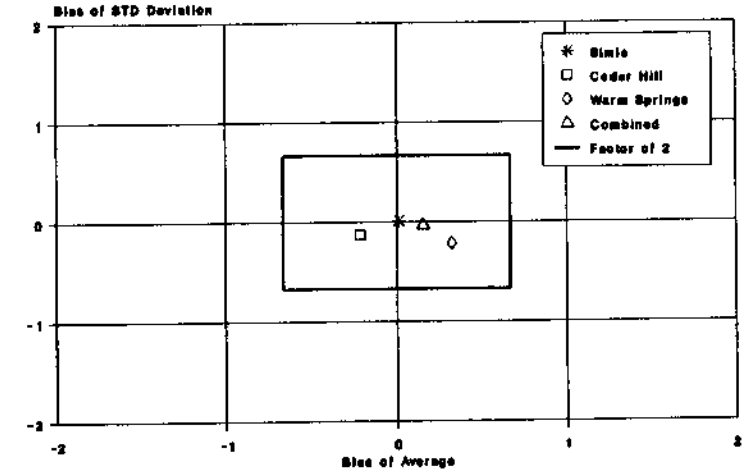

Qs = 7.1e-7*(ws-18)^3
Background Based on Lee Vining
Negative Bias Implies Overprediction

Cox Screening Test Results
ISC, GBUAPCD Emission Factor

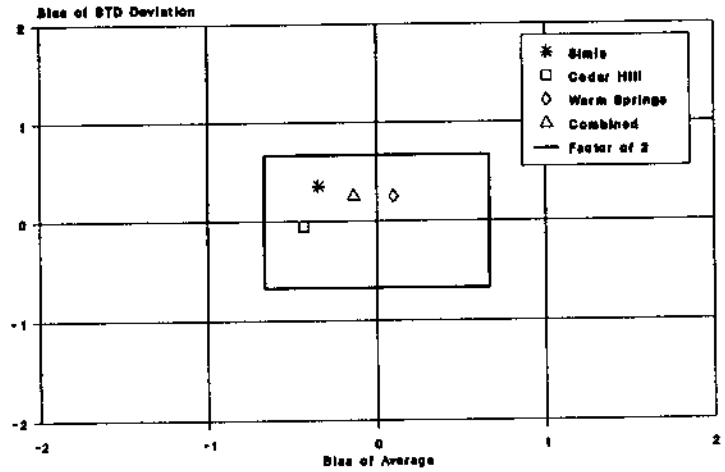

Qs = 9.36e-6*exp(.13ws)
Background Based on Lee Vining
Negative Bias Implies Overprediction

Cox Screening Test Results
ISC, MRI Emission Factor

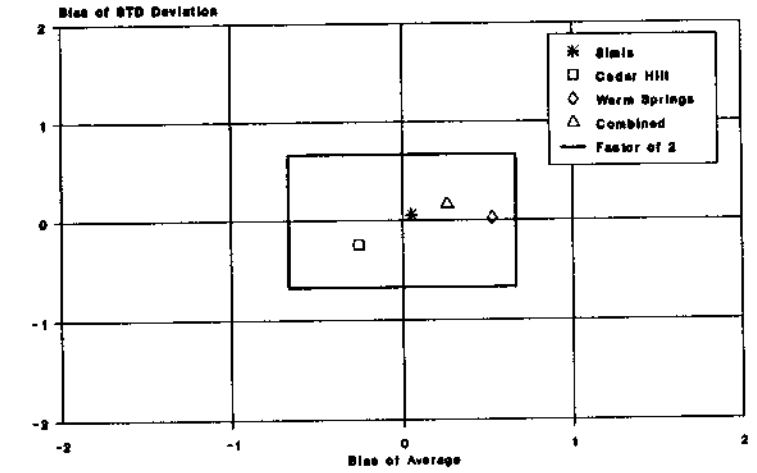

Qs = 7.1e-7*(ws-18)^3
Background Based on Lee Vining
Negative Bias Implies Overprediction

Figure 4-2

For the combined Mono Lake data set, FDM with either emission factor relationship tended to have the slightly better statistical performance measures based on a lower overall scatter and the ability to better predict the RHC and fractional bias of the standard deviation. Although the differences were slight, in nine out of ten instances FDM had better statistics than ISCST for the overall data set. With respect to ISCST, FDM generally predicted higher more variable PM_{10} concentrations which compared more favorably with the observations. There was a small tendency of both models to underpredict the highest PM_{10} concentrations.

The GBUAPCD empirical emission factor slightly outperformed the MRI cubic wind speed emission algorithm for six out of ten performance statistics for the combined Mono Lake data set. The MRI based approach tended to underpredict the observations, while the GBUAPCD method overpredicted the mean. The MRI wind-blown PM_{10} emission relationship had considerably more scatter, with a NMSE greater than one when either dispersion model was employed.

For the data sets comprised of the observations from individual stations, the results of the evaluation were mixed with different emission algorithms and models performing better for different sites. At the Warm Springs and Cedar Hills stations FDM had the edge, while at Simis ISCST had the better performance statistics. At Simis and especially at Warm Springs, FDM predicted higher more variable PM_{10} concentrations than ISCST for both emission factor methods. At Warm Springs some of the model differences could be attributed to manner in which the area sources were configured for ISCST. The sensitivity tests in Appendix B indicated that for receptors close to large area sources, that ISCST's area source routine can predict artificially low values whenever the source is not sufficiently subdivided or if winds cross the area source at an angle. At Cedar Hill, the effects of plume depletion which caused relatively greater mass to be removed when the FDM model was employed, started to become important and ISCST predicted higher values than FDM. However, these differences were masked by the relatively large average background portion (15 $\mu g/m^3$ or 50% on average) of the predictions at Cedar Hill.

A station by station comparison of the emission algorithms also provides a mixed indication of the better performing method. For the Simis and Cedar Hill data set, the MRI emission routine had the better statistics with the exception of the tendency to overpredict the highest concentrations at Simis. However at Warms Springs, the MRI cubic wind speed relationship underpredicted two of the episodes leading to a large degree of scatter and overall underprediction at this location. The GBUAPCD technique overpredicted that average PM_{10} concentration at all stations except at Warm Springs when ISCST was performing the simulations.

The discussion above focuses on comparison of the performance measures without regard to the uncertainties caused by the small sample sizes and whether the differences between the models and emission factors were statistically significant. The statistical significance of differences exhibited between the performance measures calculated for each model depend on the characteristics of the data sets and

on sample size. Statistical uncertainty was assessed using confidence limits based on the moment bootstrap resampling method as discussed in Section 3.2.2.

Figure 4-3 displays the uncertainty in the fractional bias of the mean measure by sample location and by model/emission factor combination. The large confidence limits can be attributed to dependence of the performance statistics on several key sampling periods. With the GBUAPCD emission factor, both FDM and ISCST tend to overpredict the mean of the observations and the degree of ovepredlction was significant at the Simis and Cedar Hill stations. At Warms Springs, the fractional biases were not significantly different than zero due to the large degree of statistical uncertainty in this data set. The MRI emission factor with either FDM or ISCST showed a tendency towards underprediction at all stations except Cedar Hill, but underprediction was not significant at the 95% confidence interval for any of the stations.

Table 4-2 provides a comparison of model/emission factor performance and indicates which model had the better statistical measure. The summary in this table also provides an indication of whether the differences between the models/emission factors were statistically significant at the 90% confidence level. When the statistical significance of the differences between the model/emission factors were assessed, it became apparent that the small data set sample sizes made it difficult to favor one methodology over another. For example, the linear correlation coefficients were not different from one another at the 90% level for any of the data sets. FDM tended to significantly outperform ISCST, especially when the MRI emission factor relationship was employed and provided a better indication of the highest PM_{10} concentrations for the data set as a whole. However, FDM provided no significant statistical improvement over ISCST in reducing the scatter of the predictions with the observations.

The differences between the wind-blown PM_{10} emission factor relationships were only statistically significant for 6 of the 36 possible categories in Table 4-2. The MRI technique had a significantly lower fractional bias of the mean at the Simis station, but due to the relatively large scatter produced by the MRI emission factor at Warms Springs, the NMSE statistical measure favored the GBUAPCD algorithm.

4.3 Discussion

There were many factors and assumptions in this study that could have had an important influence on the results of the performance evaluation. The results of the simulations were more dependent on the wind-blown PM_{10} emission predictions and on the configuration of the area sources than on dispersion model selection. During the study it became apparent that for the windy conditions simulated at Mono Lake, FDM and ISCST predicted similar PM_{10} concentrations with the exception that ISCST's area source routine behaved unreasonably close to the edge of the source. The critical receptors of Warm Springs and Simis were not sufficiently downwind to demonstrate whether the more sophisticated plume depletion routines in FDM produced better model performance. PM_{10} concentrations at Cedar Hill were much lower and background considerations masked differences between ISCST and FDM.

Table 4-2. Comparison of Model Performance

		Better Statistical Performance				
Model, Emission Factor	Data Set	F_bias of mean	F_bias of STD	F_bias of RHC	NMSE	Linear Corr. Coef.
FDM vs ISCST, GBUAPCD	All Stations (42 samples)	ISCST	FDM	FDM	FDM	FDM
	Simis Station (22 samples)	ISCST	FDM	ISCST	ISCST	ISCST
	Cedar Hill Station (10 samples)	FDM	FDM	NA	FDM	FDM
	Warm Springs Station (9 samples)	ISCST	FDM	NA	FDM	FDM
FDM vs ISCST, MRI	All Stations (42 samples)	FDM	FDM	FDM	FDM	FDM
	Simis Station (22 samples)	FDM	FDM	ISCST	FDM	ISCST
	Cedar Hill Station (10 samples)	FDM	FDM	NA	FDM	FDM
	Warm Springs Station (9 samples)	FDM	ISCST	NA	FDM	FDM
FDM, GBUAPCD vs MRI	All Stations (42 samples)	MRI	MRI	MRI	GBUAPCD	GBUAPCD
	Simis Station (22 samples)	MRI	MRI	GBUAPCD	MRI	MRI
	Cedar Hill Station (10 samples)	MRI	GBUAPCD	NA	MRI	MRI
	Warm Springs Station (9 samples)	GBUAPCD	GBUAPCD	NA	GBUAPCD	GBUAPCD
ISCST, GBUAPCD vs MRI	All Stations (42 samples)	GBUAPCD	MRI	GBUAPCD	GBUAPCD	GBUAPCD
	Simis Station (22 samples)	MRI	MRI	GBUAPCD	MRI	MRI
	Cedar Hill Station (10 samples)	MRI	GBUAPCD	NA	MRI	MRI
	Warm Springs Station (9 samples)	GBUAPCD	GBUAPCD	NA	GBUAPCD	GBUAPCD

Note: RHC based on top 10 samples
GBUAPCD emissions from Qa(g/m2/s) =9.35e-6*exp(.13*ws(mph))
MRI emissions from Qa(g/m2/s) =7.1e-7*(ws(mph)-18) ^ 3
Non-shaded model or emission factor was significant at 90% level.

Uncertainty in Mean Bias by Location
FDM & ISC with GBUAPCD Emission Factor

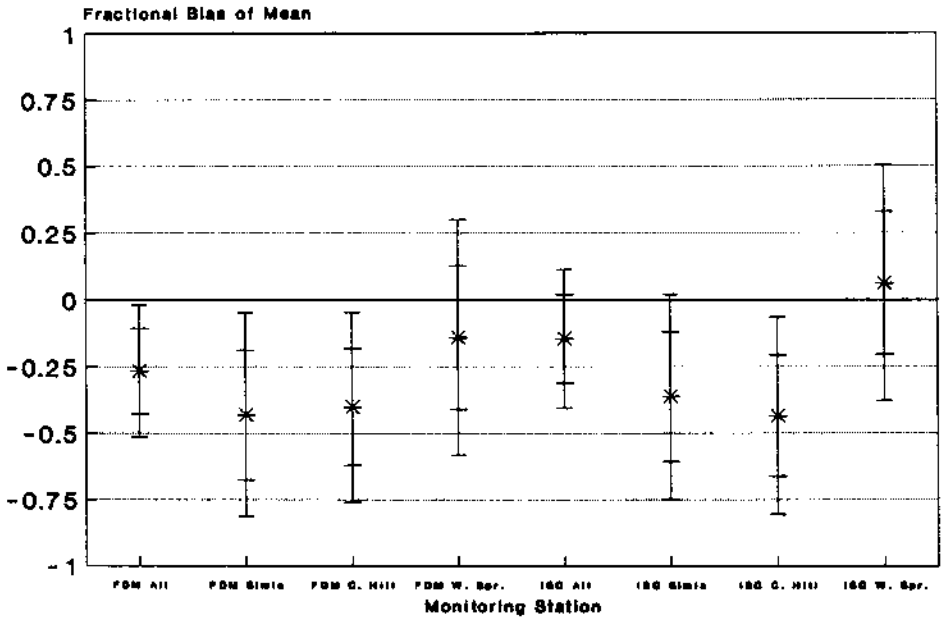

95 & 80 % Confidence Limits Shown
Qa = 9.35e-8*exp(.13*ws)
Negative Bias Implies Overprediction

Uncertainty in Mean Bias by Location
FDM & ISC with MRI Emission Factor

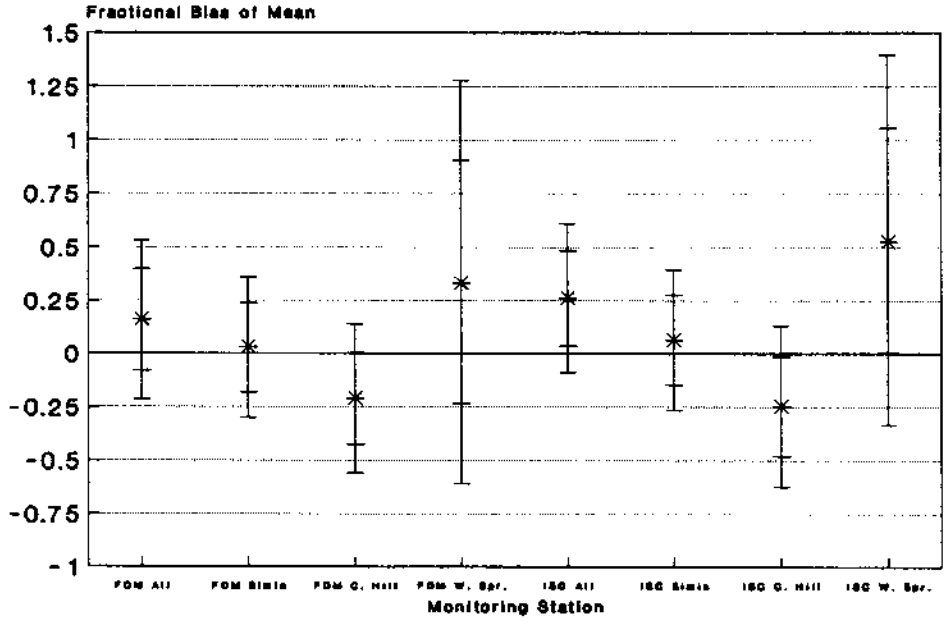

95 & 80 % Confidence Limits Shown
Qa = 7.1e-7*(ws-16)^3
Negative Bias Implies Overprediction

Figure 4-3

Assumptions concerning source to receptor orientation influenced the dispersion model simulations. Contour plots constructed from FDM simulations of PM_{10} emissions predicted by the GBUAPCD algorithm are displayed in Figures 4-4, 4-5, and 4-6, for the respective episodes 4/21/89, 5/23/90, and 5/08/91. The contour plots indicate the sharp gradients in PM_{10} predictions with both crosswind and downwind distance from the sources areas. The crosswind gradients were especially pronounced near the Warm Springs and Simis stations and moving, reducing, or extending the source area boundaries altered model predictions at these locations. For example, moving the source area along the north shore of Mono Lake 200 m to the east, reduced predictions at Simis by a factor-of-two for several of the episodes. Predictions at Warm Springs were especially sensitive to wind direction and to the east/west extent of the nearby playas. Better placement of the eroding playas which vary annually and seasonally may have improved the model predictions for several of episodes. In addition, predictions at Warm Springs, which were sensitive to wind direction, may have been improved by using local wind data. The application of local wind data at the Warms Springs monitor may also change the emission estimates and help explain the poor performance of the MRI algorithm when compared to the GBUAPCD method.

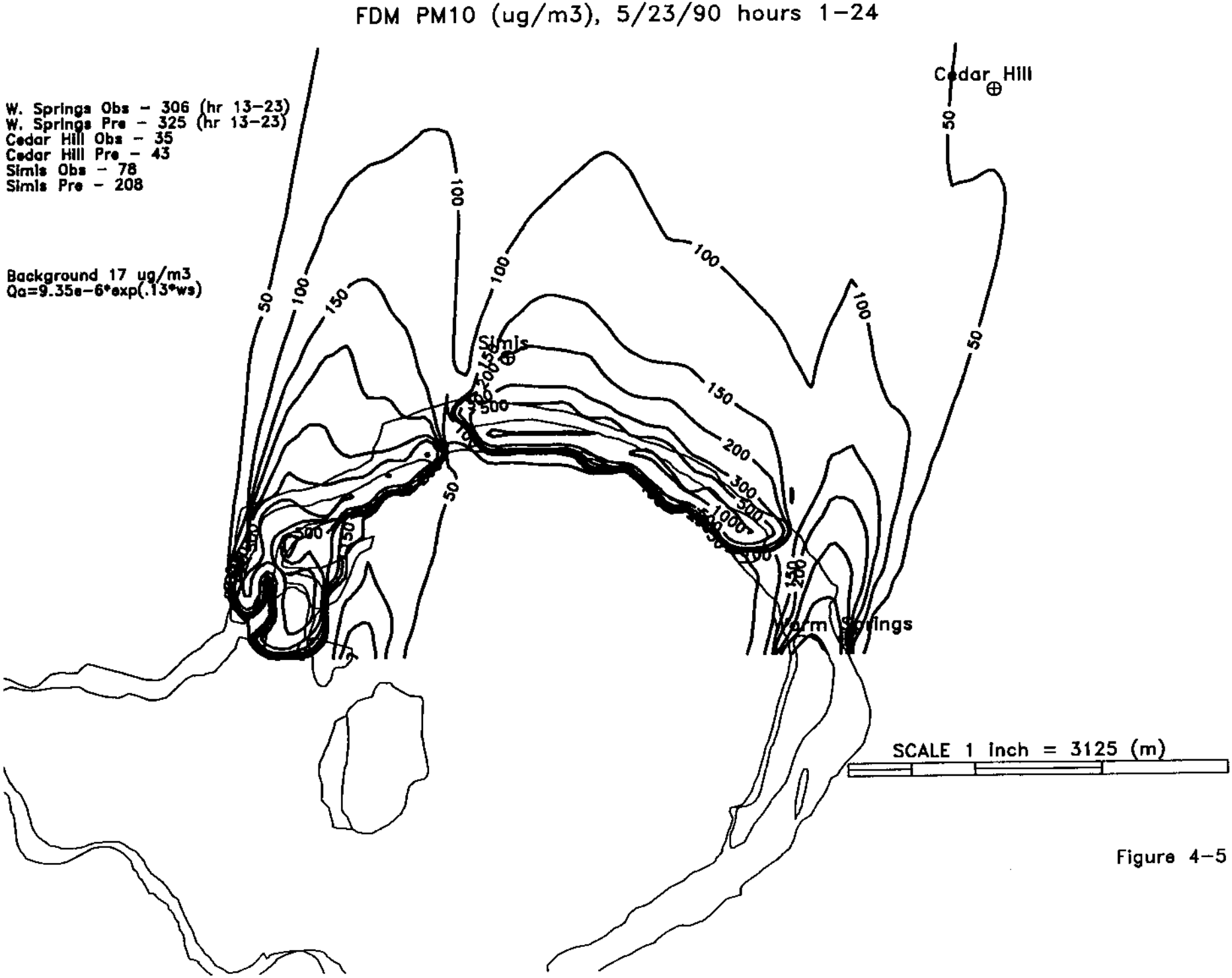
FDM PM10 (ug/m3), 5/23/90 hours 1-24
W. Springs Obs - 306 (hr 13-23)
W. Springs Pre - 325 (hr 13-23)
Cedar Hill Obs - 35
Cedar Hill Pre - 43
Simis Obs - 78
Simis Pre - 208
Background 17 ug/m3
Qa=9.35e-6*exp(.13*ws)
Cedar Hill
Simis
Warm Springs
SCALE 1 inch = 3125 (m)

Figure 4-5

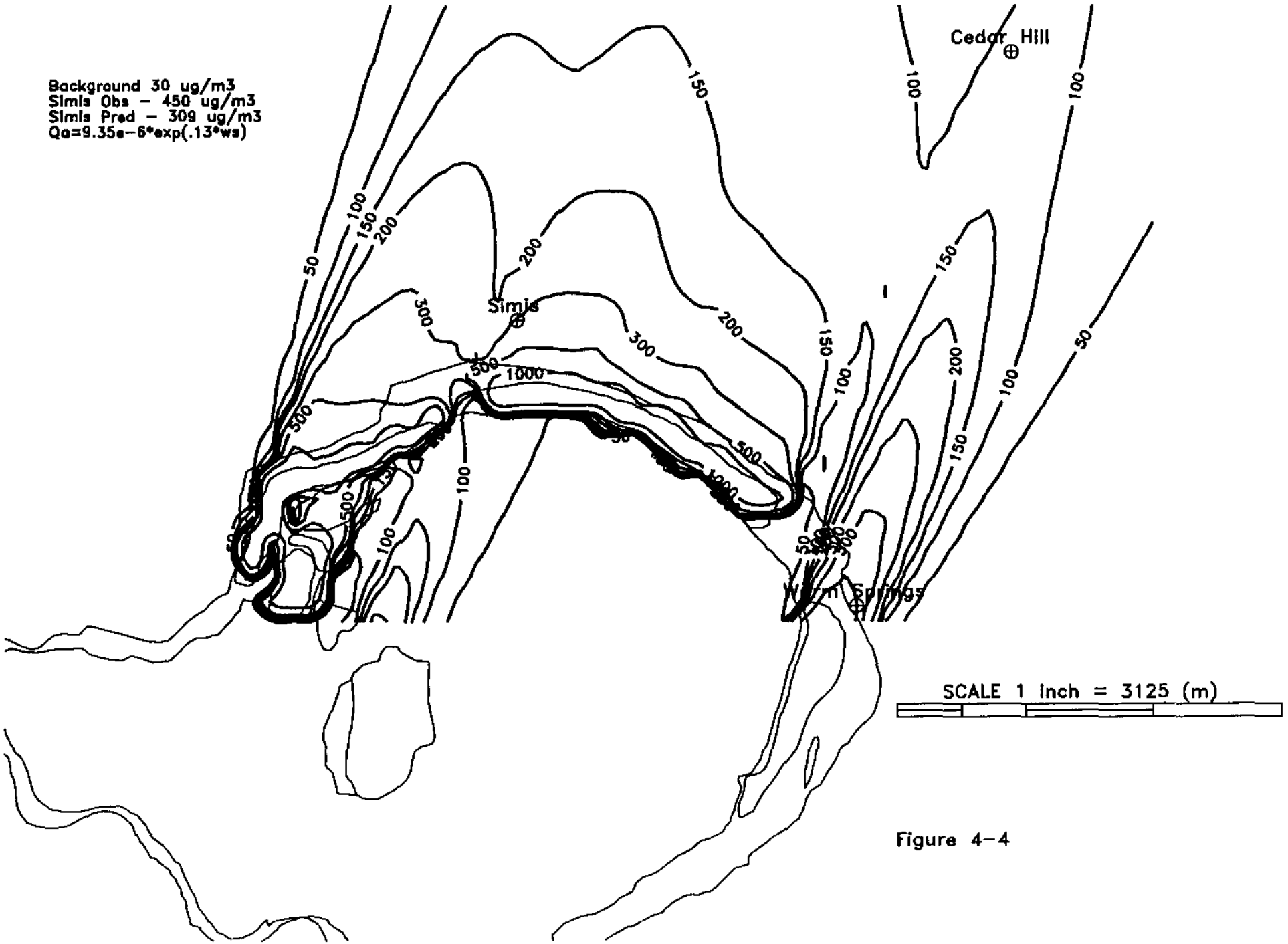
FDM PM10 (ug/m3), 4/21/89 hours 11-23
Background 30 ug/m3
Simis Obs - 450 ug/m3
Simis Pred - 309 ug/m3
Qa=9.35e-6*exp(.13*ws)
Cedar Hill
Simis
Warm Springs
SCALE 1 inch = 3125 (m)

Figure 4-4

FDM PM10 (ug/m3), 5/08/91 hours 1-24

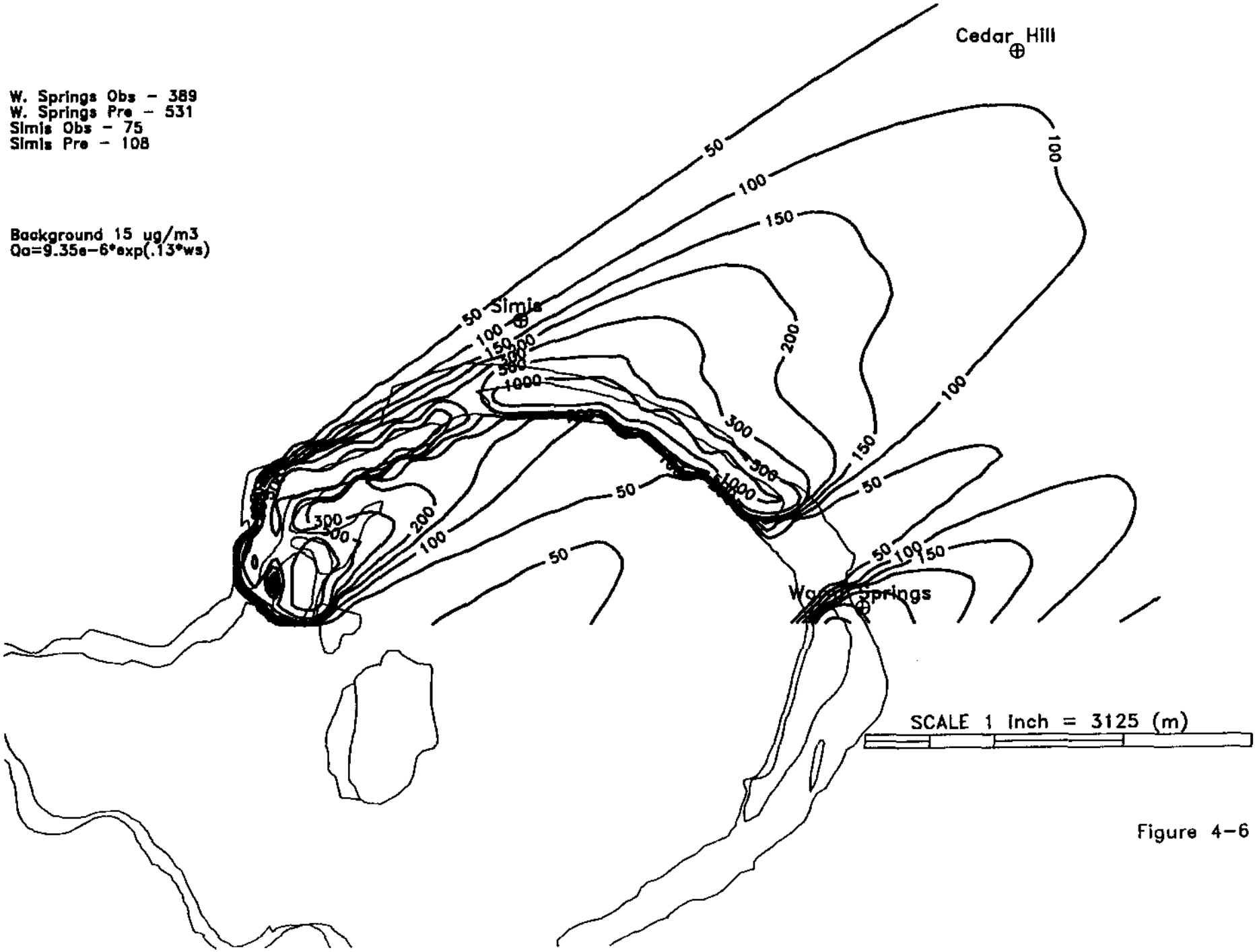

Figure 4-6

5.0 Summary

The Mono Lake Air Quality Model Evaluation Study evaluated dispersion modeling techniques for the simulation of wind-blown PM_{10} emissions from the exposed shores of Mono Lake. Two emission algorithms and two dispersion models were evaluated using PM_{10} and meteorological data collected at locations near Mono Lake. The dispersion models evaluated were the ISCST model which is currently recommended by both the U.S. EPA and the CARB for regulatory assessments associated with fugitive PM_{10} and FDM which has recently been developed and was specifically designed for computing concentrations and deposition fluxes from fugitive dust sources. Based on different interpretations of portable wind tunnel experiments conducted at Mono Lake, emission factor algorithms suggested by the GBUAPCD and MRI were also tested. The GBUAPCD emission factor was derived from a purely empirical fit to the wind tunnel data and the MRI method while being empirical conforms to the cubic wind speed dependency commonly found in the literature. The results of the evaluation were as follows:

- for the combined data set, either dispersion model or emission factor combination was able to predict the average, standard deviation, and Robust Highest Concentration of the PM_{10} observations within a factor-of-two and explain over 50% of the spatial and temporal variation in the observations

- FDM was found to be the technically superior model for the prediction of PM_{10} concentrations downwind of wind eroding area sources due to a more concise and easier to apply area source algorithm. The ISCST area source algorithm produced arbitrary concentrations close to large area sources that depended on the manner in which these sources were subdivided. The plume depletion routines in FDM were also favored, but for fine particles and windy conditions improvements would only be expected for receptors beyond about 10 km

- FDM outperformed ISCST for the overall data set, tending to more closely predict the higher concentrations and the variability of the PM_{10} observations. However FDM's distinction was not consistent, with ISCST performing better for some stations and performance measures

- although FDM slightly outperformed ISCST in most instances model predictions were often not different in either a statistical or a practical sense

- the MRI emission factor combined with either dispersion model algorithm significantly underpredicted two episodes at the Warms Springs station where wind speeds were in the 16 to 25 mph range and overpredicted the higher PM_{10} observations at Simis. The GBUAPCD method offered significantly less scatter than the MRI technique, but displayed a tendency to overpredict the mean value of the observations

- the predictions for both dispersion models and emission factor techniques at the Warms Springs and Simis monitoring stations were heavily influenced by the specification of the eroding area source boundaries. Slight changes in the spatial extent of these area sources or small changes in wind direction had the potential to significantly alter the model predictions at these two locations.

On basis of the technical comparison, sensitivity analysis and the slightly better ability to duplicate ambient PM_{10} concentrations, the study recommends that FDM be employed in future simulations of wind-blown PM_{10} emissions at Mono Lake. The distinction between the emission factors in the performance evaluation was less clear and probably less important that the knowledge concerning the location and extent of the eroding areas. For conservative regulatory applications, the GBUAPCD technique yielded the higher average values while the MRI method produced the higher 24-hour PM_{10} concentrations.

6.0 References

Arya, S. P., 1988. Introduction to Micrometeorology. Academic Press, Inc., San Diego, CA, 92101.

CARB, 1989. Reference Document for California Statewide Modeling Guideline. California Air Resources Board, Sacramento, CA, April, 1989.

Cowherd, C., 1991a. Wind Erosion Emission Factors for Mono Lake. Memorandum from Chat Cowherd, MRI, to Duane Ono, GBUAPCD, April 29, 1991.

Cox, W.G, 1990. Mono Lake Group II PM_{10} Monitoring Update. Greater Basin Unified APCD, 157 Short Street, Suite 6, Bishop, CA 93514, June 8, 1990.

Cox, W.M., 1987. Protocol for Determining the Best Performing Model. U.S. EPA, Monitoring and Data Analysis Division, Source Receptor Analysis Branch, September, 1987.

Gillette, D.A., Blifford, I.H., and D.W. Fryrear, 1974. The Influence of Wind Velocity on the Size Distributions of Aerosols Generated by the Wind Erosion of Soils. J. of Geo. Res., Vol 79, pp 4068-4075.

Hanna, S.R., 1989. Confidence Limits for Air Quality Model Evaluations, As Estimated by Bootstrap and Jackknife Resampling Methods. Atmos. Envir., Vol 23, pp 1385-1398.

Holzworth, G.C., 1972. Mixing Heights, Wind Speeds, and Potential for Urban Air Pollution Throughout the Contiguous United States. U.S. EPA, Office of Air Programs, Research Triangle Park, NC 27711, Publications No. AP-101.

Ono, Duane, 1991. Wind Erosion Algorithm for PM_{10} Emissions from Mono Lake. Memorandum from Duane Ono, GBUAPCD to Chat Cowherd, MRI, May 9, 1991.

Pye, K., 1987. Aeolian Dust and Dust Deposits. Academic Press, Inc., Orlando, FL 32887.

TRC Environmental Consultants, Inc., 1990. Revised Data Report: Deposition Model Evaluation, Bunker Hill RI/FS. Prepared for Dames & Moore, 1125 17th St, Suite 1200, Denver, CO 80202, Dames & Moore Report No. 15852-065/PD193/45030, December 5, 1990.

TRC Environmental Consultants, Inc., 1991. Air Quality Modeling Protocol: Mono Lake Evaluation Study. Prepared for the Greater Basin Unified APCD, 157 Short Street, Suite 6, Bishop, CA 93514, May 15, 1991.

Turner, D.B., 1970. Workbook of Atmospheric Dispersion Estimates. U.S. EPA, Office of Air Programs, Research Triangle Park, NC 27711, AP-42.

U.S. EPA, 1978. Workbook for Comparison of Air Quality Models. U.S. EPA, Office of Air Quality Planning and Standards, Research Triangle Park, NC 27711, EPA-450/2-78-028a.

U.S. EPA, 1984. Interim Procedures for Evaluating Air Quality Models (Revised). U.S. EPA, Office of Air Quality Planning and Standards, Research Triangle Park, NC 27711, EPA-450/4-84-023.

U.S. EPA, 1985. Interim Procedures for Evaluating Air Quality Models. Experience with Implementation.U.S. EPA, Office of Air Quality Planning and Standards, Research Triangle Park, NC 27711, EPA-450/4-85-006.

U.S. EPA, 1986a. Guideline on Air Quality Models, Revised Edition. U.S. EPA, Office of Air Quality Planning and Standards, Research Triangle Park, NC 27711, EPA-450/2-78-027R.

U.S. EPA, 1986b. MPDA-1. Meteorological Processor for Diffusion Analysis - User's Guide. EPA, Office of Research and Development, Research Triangle Park, NC 27711, EPA/600/8-86-011.

U.S. EPA, 1987a. Industrial Source Complex (ISC) Dispersion Model Users's Guide. - Second Edition (Revised), Volume I. U.S. EPA, Office of Air Quality Planning and Standards, Research Triangle Park, NC 27711, EPA-450/4-88-002a.

U.S. EPA, 1987b. On-Site Meteorological Program Guidance for Regulatory Modeling Applications. U.S. EPA, Office of Air Quality Planning and Standards, Research Triangle Park, NC 27711, EPA-450/4-87-013.

U.S. EPA, 1989. Air/Superfund National Technical Guidance Study Series, Volume IV - Procedures for Dispersion Modeling and Air Monitoring for Superfund Air Pathway Analysis, Interim Final. U.S. EPA, Office of Air Quality Planning and Standards, Research Triangle Park, NC 27711, EPA-450/1-89-004.

Winges, K.D., 1990. User's Guide for the Fugitive Dust Model (FDM) (Revised). U.S. EPA Region 10, 1200 Sixth Ave, Seattle, WA 98101, EPA-910/9-88-202R.